Characterisation of NagA and NagB from methicillin-resistant *Staphylococcus aureus*

A thesis submitted in partial fulfilment of the

requirements for the degree of

Master of Science in Biochemistry

in the School of Biological Sciences

by James Sandwell Davies

University of Canterbury

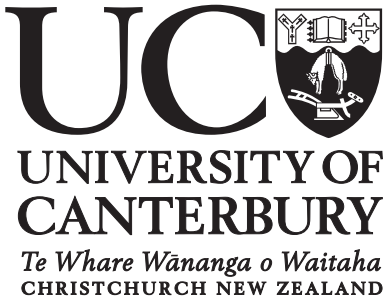

March 2017

Abstract

The principal aim of this thesis is to build an understanding of how amino sugars are metabolised in a clinically relevant strain of *Staphylococcus aureus*. Amino sugars, such as sialic acid and *N*-acetylglucosamine, are prevalent mucosal sugars that are incorporated into glycoconjugates attached to mucosal cell surfaces. Specifically, the amino sugars can be scavenged from host glycoconjugates and metabolised by bacterial pathogens as a nutrient source. *Staphylococcus aureus* possesses the enzymatic machinery to scavenge host-derived host-derived amino sugars from their surrounding environment and utilise them as sources, of carbon, nitrogen and cell wall precursors.

A number of amino sugar metabolic pathways converge upon two enzymes, *N*-acetylglucosamine-6-phosphate deacetylase, NagA, and glucosamine-6-phosphate deaminase, NagB. These enzymes catalyse the utilisation steps of these pathways, directing metabolites into either peptidoglycan biosynthesis or glycolysis. Due to this central role in the metabolism of host-derived nutrients, understanding of the structure, function and any patterns for regulation of these enzymes will inform the development of new antibiotic and therapeutic strategies.

The structure and function of NagA and NagB from methicillin-resistant *S. aureus* were investigated in this thesis. This constitutes the first biophysical characterisation of these enzymes from *S. aureus*. Structural data show that both of these enzymes adopt a dimeric architecture in solution, which is a novel arrangement in the case of NagB. Kinetic analyses detail the catalytic capabilities of both enzymes, and suggest two different patterns of regulation that may influence the activity of these enzymes *in vivo*.

Overall, these experiments add to the understanding of how amino sugars are utilised by *S. aureus*, and provide a basis for further research into NagA and NagB structure, function and regulation.

Acknowledgements

Firstly, special thanks to my supervisor Renwick Dobson for his sound scientific guidance, and for encouraging me to develop independence as a researcher. Thanks also to my associate supervisor Grant Pearce for his assistance in the lab and tolerance of my often repetitive questions about how to 'do science'. I'd like to also especially acknowledge Rachel North, for her mentorship this year, and advice on all matters to do with my research.

Thanks to everyone in the Dobson and Pearce lab groups, I have thoroughly enjoyed working alongside each and every one of you, and look forward to doing so in the future. In particular, thanks to Chris, Jen, Serena and Jenna for showing me the ropes in the lab, and for the laughs along the way. Thank to William, Cameron and Hamish for hanging in there with me for the last two years. A special mention also to David for your enthusiasm and insight into my project.

Finally, thanks to my friends and family for supporting me and my passion for science.

Table of contents

Abbreviations

[*S*]	substrate concentration
°C	degree celcius
Å	angstroms
AUC	analytical ultrcentrifugation
c(M)	continuous mass distribution
c(s)	continuous sedimentation coefficient distribution
C3	Collaborative Crystallisation Centre
CA-MRSA	Community-associated methicilin resistant *Staphylococcus aureus*
Da	dalton
D_{max}	maximum interatomic distance
DTT	dithiothreitol
f/f0	frictional ratio
Fru-6-P	fructose-6-phosphate
G6PDH	glucose-6-phosphate dehydrogenase
GlcN	glucosamine
GlcNAc	N-acetylglucosamine
GlmS	glucosamine-6-phosphate synthase
IPTG	isopropyl β-D-1-thiogalactopyranoside
k_{cat}	catalytic turnover number
kDa	kilodalton
K_i	inhibition constant
K_m	Michaelis -Menten constant
LB	luria bertani
M	molar
mg	milligram
mL	millilitre
mM	millimolar

MRSA	methicillin-resistant *Staphylococcus aureus*
MurNAc	*N*-acetylmuramic acid
MurQ	*N*-acetylmuramic acid 6-phsophate etherase
NADP+	nicotinamide adenine dinucleotide
NADPH	nicotinamide adenine dinucleotide, reduced form
NagA	*N*-acetylglucosamine-6-phosphate deaminase
NagB	glucosamine-6-phosphate deaminase
nL	nanolitre
Neu5Ac	*N*-acetylneuraminic acid (sialic acid)
OD_{600}	optical density at 600 nm
P(r)	distance distribution function
PDB	protein data bank
PGI	phosphoglucoisomerase
PTS	phosphotransferase system transporter
R_g	radius of gyration
R_I	refractive index
rpm	revolutions per minute
s	second
S	sedimentation coefficient, Svedberg
SAXS	small angle x-ray scattering
Tris	2-amino-2-hydroxymethyl-propane-1,3-diol
TCEP	tris(2-carboxyethyl)phosphine
V	initial velocity
v/v	volume to volume
w/v	weight to volume
µg	microgram
µL	microlitre
µM	micro

Chapter One:

Introduction

1.1 Bacterial pathogens have evolved specific pathways to utilise host-derived nutrients

Many species of pathogenic bacteria have evolved metabolic pathways to utilise a wide array of compounds as nutrient sources, often reflecting the availability of nutrients their niche (Plumbridge, 2015). Mammals are a rich source of nutrients—particularly throughout the mucosal surfaces of the gastrointestinal tract and respiratory system, where there are an abundance of sugars, amino acids and nitrogen containing compounds (Rohmer, Hocquet, & Miller, 2011). Amino sugars, such as sialic acid and *N*-acetylglucosamine, are prevalent in mucosal surfaces, particularly in the sugar chains of the heavily glycosylated mucin proteins (McDonald, Lubin, Chowdhury, & Boyd, 2016). An amino sugar is defined as a carbohydrate where a hydroxyl at carbon two is replaced by an amine group, or in some cases a more complex nitrogen-containing functional group (Salton, 1964). Amino sugars can become available to pathogens as nutrient sources through the action of neuraminidase and glucosaminidase enzymes, which catalyse the cleavage of sugars from glycoconjugates. These enzymes are either produced endogenously by the host, or secreted by the pathogens/other commensal bacteria into the extracellular milieu (Vimr, 2013).

In bacteria that possess the necessary enzymes to import and process amino sugars, metabolism ultimately converges on two enzymes: *N*-acetylglucosamine-6-phosphate deacetylase (NagA), and glucosamine-6-phosphate deaminase (NagB). These enzymes catalyse sequential reactions, yet each product can be fed into major metabolic pathways; the product of NagA, glucosamine-6-phosphate, can be fed into peptidoglycan biosynthesis, while the product of NagB, fructose-6-phosphate, is a glycolytic substrate (Plumbridge, 2015).

Specialised metabolic pathways are hypothesised to provide pathogenic bacteria a competitive advantage over resident commensal flora in the host (Rohmer et al., 2011). As pathogenic bacteria often derive their carbon and energy from a host, the regulation of the virulence determinants is often controlled by nutrient availability (Somerville & Proctor, 2009). Thus, it is likely that complex interplay exists between specialised bacterial metabolism, pathogenesis, colonisation and disease potential. The ability to metabolise amino sugars has indeed been linked to these processes in a number of bacteria, such as *Escherichia coli* and *Vibrio cholerae*, where sialic acid catabolism is thought to confer a competitive advantage during intestinal colonisation (Huang, Chassard, Hausmann, von Itzstein, & Hennet, 2015; McDonald et al., 2016).

1.2 Focus

This thesis focuses on the NagA and NagB enzymes from *Staphylococcus aureus. S. aureus* is a pathogenic, gram-positive bacterium that frequently colonizes mucosal surfaces in humans, and is responsible for a large range of serious infections. Although historically associated with infections caused in the healthcare setting, infections caused by community-associated methicilin-resistant *S. aureus* (CA-MRSA) are now reaching epidemic level (David & Daum, 2010). MRSA strains are now resistant to all β-lactam antibiotics, and are rapidly evolving and proliferating resistance to new antibiotics, such as vancomycin (David & Daum, 2010). New, non-conventional therapeutic strategies, as well as novel antibiotic development are needed to treat these infections.

NagA and NagB have been described as a 'gate' that controls the distribution of amino sugars in *S. aureus* (Komatsuzawa et al., 2004). It is anticipated that the structural and biophysical characterisation of NagA and NagB presented here will aid in understanding of the function and possible regulation of this 'gate' in an antibiotic resistant strain, and provide a basis for examining these enzymes as therapeutic targets. Our research group has already studied a number of enzymes in the sialic acid catabolic pathway (North et al., 2014) – the work presented in this thesis is a continuation of the characterisation of this pathway. The enzymes studied here originate from the CA-MRSA strain USA300_TCH1516. This strain was isolated

from a patient with severe sepsis syndrome, and was found to be highly similar to other MRSA strains based on whole-genome alignments (Highlander et al., 2007). Throughout this thesis, this strain is referred to simply as MRSA. Additionally, the term amino sugar is used in reference to four of the most common sugars that are thought to be metabolised by *S. aureus*: sialic acid, *N*-acetylglucosamine (GlcNAc), glucosamine (GlcN) and *N*-acetylmuramic acid (MurNAc), as shown in Fig. 1. Sialic acid here refers to the most common form, *N*-acetylneuraminic acid or Neu5Ac, although it should be noted that the sialic acids encompass a number of different nine carbon keto sugars (Vimr, 2013).

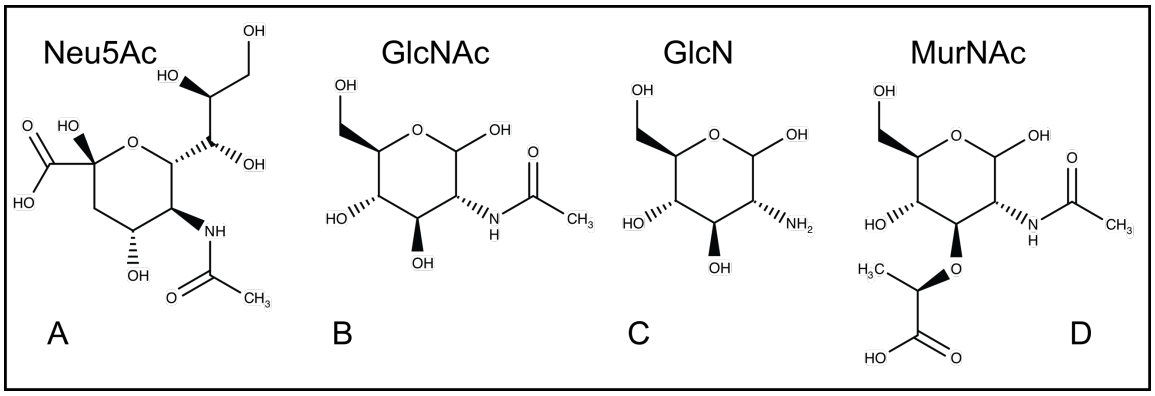

Figure 1. Chemical structures of amino sugars. A, *N*-acetylneuraminic acid; B, *N*-acetylglucosamine; C, glucosamine; D *N*-acetylmuramic acid. Structures show a characteristic nitrogen-based moiety at carbon two.

1.3 Evidence for amino sugar metabolism in S. aureus

The nasal mucosa of the anterior nares is the main ecological niche of *S. aureus*, although other areas of the body can be colonised, such as the gastrointestinal tract (Gordon & Lowy, 2008). Here we speculate that *S. aureus* will encounter free amino sugars in the nasal mucosa, considering their ubiquity in glycoconjugates, and the presence sialidases of nasopharynx produced by pneumococcal species (Owen et al., 2015). *S. aureus* itself produces *N*-acetylglucosaminidases that are either membrane-associated, or secreted into the milieu, so it is likely that *S. aureus* has ready access to bound amino sugars (Alvarez-Anorve et al., 2016) To date, physiological concentrations of the amino sugars in the nasal mucosa are unknown.

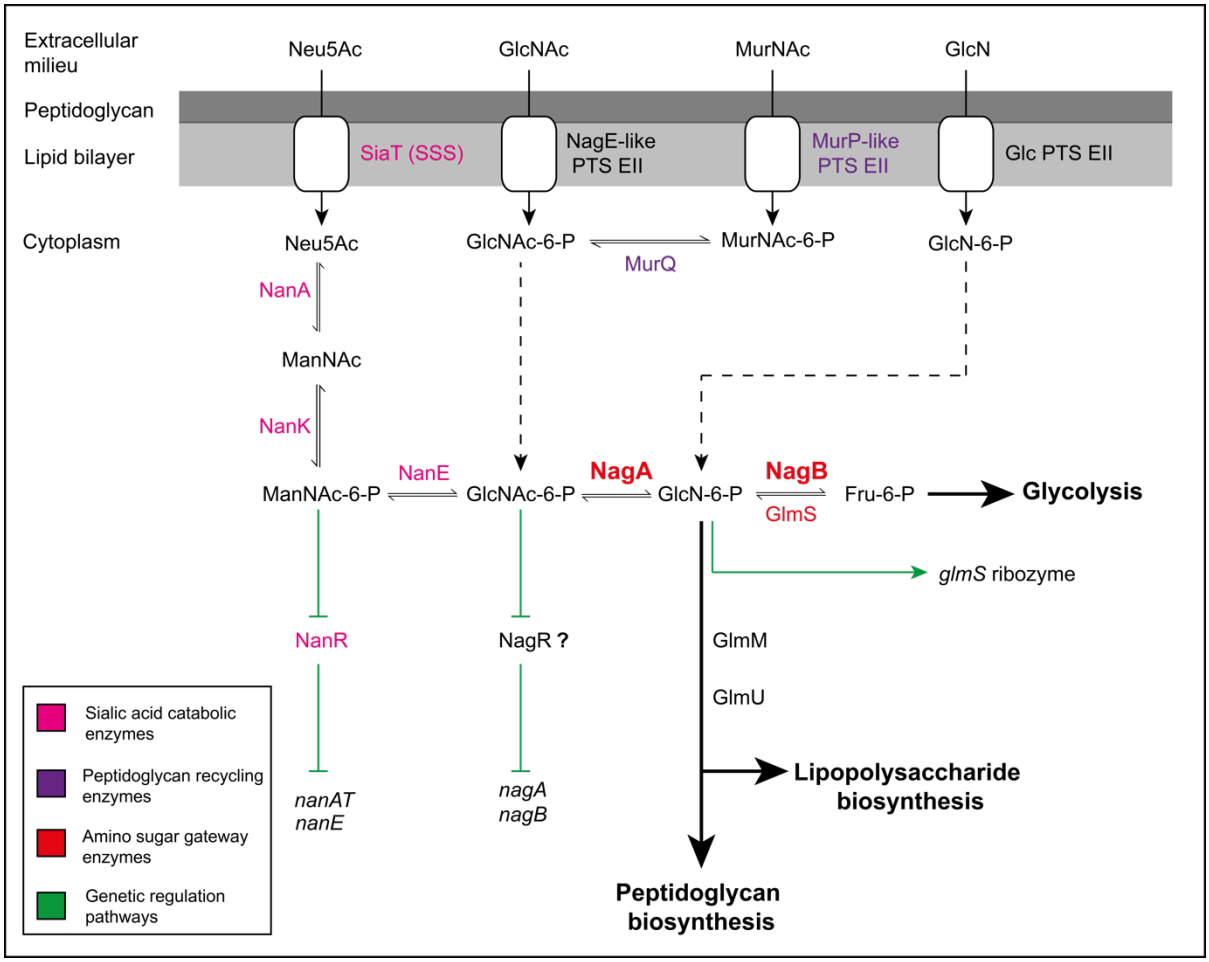

Figure 2. Proposed amino sugar uptake and utilisation pathway in MRSA. Import into the cell is catalysed by phosphotransferase system (PTS) transporters, aside from sialic acid, which is transported *via* a sodium solute symporter (SSS), SiaT. Pink shows the enzymes in the sialic acid enzyme pathway, as first identified by Olson, King, Yahr, and Horswill (2013). Purple shows the recently identified proteins of the peptidoglycan recycling pathway (Borisova et al., 2016) In red are the amino sugar gateway enzymes. Green shows genetic regulation pathways. The NanR and the GlmS ribozyme modes of genetic regulation have been demonstrated *in vitro* (Lunse, Schmidt, Wittmann, & Mayer, 2011; Olson et al., 2013) yet the action of NagR shown here is speculative. This proposed pathway is based on those established in *E. coli* and *Bacillus subtilis* (Plumbridge, 2015) and *S. aureus* (Komatsuzawa et al., 2004), as well as curated KEGG genome data (Kanehisa, Sato, Kawashima, Furumichi, & Tanabe, 2016).

It has been shown *in vitro* that *S. aureus* can utilise sialic acid as a carbon source, and is equipped with both the *nan* and *nag* genes necessary for the catabolic pathway (Olson et al., 2013). As shown in Fig 2., this involves transport through a dedicated membrane transporter, SiaT; followed by the action of a lyase, NanA; which releases *N*-acetylmannosamine and pyruvate; a kinase, NanK, which phosphorylates mannosamine; and an epimerase, NanE, which epimerises *N*-acetylmannosamine-6-phosphate (ManNAc-6-P) to *N*-acetylglucosamine-6-phosphate (GlcNAc-6-P), the substrate of NagA.

This pathway is genetically regulated through the action of the NanR repressor proteins, which represses the *nanAT* and *nanE* genes. This repression is alleviated *in vitro* by ManNAc-6-P, one of the intermediate metabolites in the pathway (Olson et al., 2013). The *nagA*, *nagB* and *nagE* genes are thought to be regulated in a similar fashion, although this is yet to be established in *S. aureus.*

Activity of *S. aureus* NagA and NagB has been demonstrated *in vivo*, where knockdown studies showed that NagA can direct exogenous amino sugars into peptidoglycan biosynthesis pathway. This study also revealed another important aspect of the 'gate'; glucosamine-6-phosphate synthase, GlmS, which catalyses the opposite reaction to NagB. In *S. aureus*, this is an important enzyme in the peptidoglycan biosynthesis pathway as it is the only biosynthetic enzyme that produces glucosamine-6-phosphate from glucose. There is great demand for peptidoglycan biosynthesis in gram-positive bacteria, and it follows that GlmS has high activity, and is potentially tightly metabolically controlled alongside NagA and NagB– if there were no elements for control of either NagB and GlmS, it is likely that there would be loss of GlcN-6-P to futile cycling between the two enzymes (Alvarez-Anorve et al., 2016; Hiramatsu, 2001). Knockouts of *nagA*, *nagB* and *glmS* the MRSA strain BB270 all showed increased susceptibility to β-lactams when grown on amino sugars, which highlights both the importance of these enzymes in distributing to peptidoglycan biosynthesis, and their potential for roles in therapeutic development (Komatsuzawa et al., 2004).

The peptidoglycan recycling pathway presents another pathway that can feed into NagA and NagB. This has recently been demonstrated as being an important metabolic process in gram-positive species, where peptidoglycan fragments shed into the growth medium are

recovered. Crucial here is the action of autolysin enzymes on peptidoglycan, which can liberate the amino sugar *N*-acetylmuramic acid (MurNAc) from peptidoglycan. After import into the cell *via* a dedicated phosphotransferase system, MurNAc-6-P can be converted back to GlcNAc-6-P by the action of MurNAc-6-P etherase (MurQ). This process has been discovered in MRSA, where an MurNAc catabolic operon has been identified (comprising a PTS, MurQ and a regulatory protein (Borisova et al., 2016). This pathway was shown to be crucial for survival of *S. aureus* during stationary phase, where approximately 5% of the cell wall was recycled (Borisova et al., 2016). This highlights the need for a functional NagA *in vivo*, which would be required as MurNAc-6-P is not fed directly back into the peptidoglycan biosynthetic pathway (Fig. 2).

1.5 Regulation of amino sugar distribution

In many organisms the expression and activity of NagA and NagB are controlled through multiple levels of regulation. GlcNAc-6-P is a key metabolite for regulation of this pathway: in *E. coli*, GlcNAc-6-P both allosterically activates NagB, and induces *nagE-BACD* expression by binding the NagC repressor protein. This allosteric activation is part of feed-forward loop that is thought to sense flux through the pathway (in terms of fluctuating metabolite concentrations), that in turn allows rapid response to external signals (Alvarez-Anorve et al., 2016). Whether or not NagB is subjected to any pattern of regulation has yet to be explored in *S. aureus*.

As alluded to previously, GlmS acts in the opposing direction to NagB. GlmS has been shown to be subject to genetic regulation in a strain of vancomycin-resistant *S. aureus*, where the 5'-UTR of *glmS* mRNA has been shown to form a metabolite-sensing riboswitch (Lunse et al., 2011). This *glmS* ribozyme catalyses is own cleavage upon glucosamine-6-phosphate binding, that eventually destabilises the mRNA molecule, lowering the production of the GlmS enzyme. This highlights the fine-tuned control applied to these enzymes.

1.5 NagA: structure and catalytic chemistry

NagA is a member of the aminohydrolase family, a group of enzymes that catalyse the cleavage of an amide bond to amino acids, nucleic acids and sugars. Aminohydrolase enzymes all share the same an $(\beta/\alpha)_8$ structural scaffold, and often bind metal ions in the active site (Hall, Brown, et al., 2007). In the forward direction, NagA catalyses the deacetylation of *N*-acetylglucosamine-6-phosphate using water to form glucosamine-6-phosphate and release acetate (Fig. 3.).

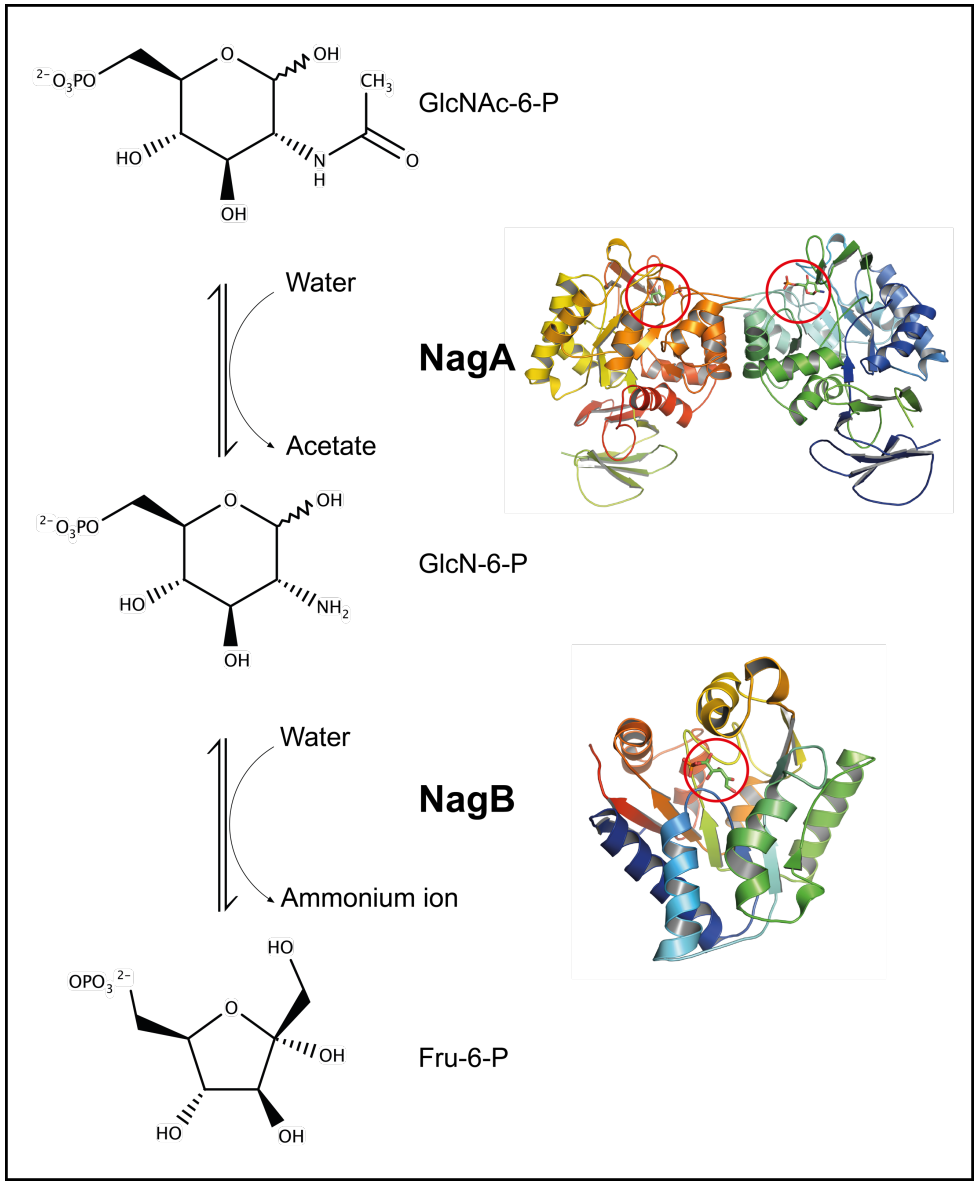

Figure 3. Deacetylation and deamination reactions catalysed by NagA and NagB. Also shown are the structures of *B. subtilis* NagA and NagB. Circled in red show the locations of the active site(s). Structures were drawn using PyMol.

Sequence data and structural evidence point to NagA being a member of the metal-dependent superfamily of aminohydrolases, utilising divalent metal ions in the active site to catalyse this deacetylation reaction. The *Bacillus subtilis* structure shows a binuclear metal centre, with two Fe^{2+} ions (Vincent, Yates, Garman, Davies, & Brannigan, 2004), whilst the *E. coli* and *Thermatoga maratima* enzymes have mononuclear metal centres (Hall, Brown, et al., 2007). The basic NagA reaction mechanism involves attack of the GlcNAc-6-P carbonyl by an activated water molecule, followed by protonation of the leaving group by, the amine of GlcN-6-P, by an invariant aspartic acid residue (Asp-273). In the mononuclear site, the metal ion is suggested to aid catalysis by polarising the carbonyl oxygen, encouraging nucleophilic attack. It is hypothesised that the activation of the amide bond, and the activation of a water molecule can be shared between the two metal ions (Hall, Brown, et al., 2007)

Accordingly, significant divergence in the active site architecture is seen between the mononuclear and binuclear enzymes—this divergence is also thought to reflect differences in catalytic mechanisms. The binuclear metal ion binding site seen in the *B. subtilis* enzyme is attributed to a dual histidine motif (HxH) at the end of β-strand 1, that is not present in *E. coli*. This motif is present in MRSA NagA, as shown in Fig. 4 (following page). Alongside the HxH motif, the residue corresponding to His-143 in *E. coli* NagA is proposed to be correlated with the overall metal ligation scheme. His-143 is hypothesised to be able to help polarize the carbonyl of GlcNAc-6-P during bond cleavage, potentially in lieu of the second metal ion. In groups of sequences that cluster with known binuclear metal centre NagA enzymes, a glutamine or a glutamic acid residue is present corresponding to His-143. As shown in Fig. 4., MRSA NagA has a glutamine at this position.

Considering this sequence alignment, I hypothesise that MRSA forms a binuclear metal ion site similar to that seen in the *B. subtilis* enzyme. The evolutionary, or catalytic implications of these divergent metal sites is unclear, although the fact that there are such clear differences in active site architecture may be beneficial in designing inhibitors for these enzymes. To date, there has been no kinetic characterisation of NagA from gram-positive species.

Little is known about the oligomeric state of NagA in organisms aside from *E. coli* and *B. subtilis. B. subtilis* NagA is predicted to oligomerise in an unusual manner, where each subunit in the homodimer protrudes into the opposite subunit, contributing residues for substrate binding. His-233 and Arg-244 form a 'pincer-like' extension from the $\beta_6\alpha_6$ loop, stabilising the phosphate moiety of the substrate. Both residues are present in the MRSA sequence, but not in the *E. coli* sequence. The *E. coli* enzyme forms a tetramer in solution, with the monomer-monomer interface also formed by loops that protrude into the active site of an opposite monomer. Aside from stabilisation of the phosphate moiety, little is reported in the literature about this unusual dimerisation process.

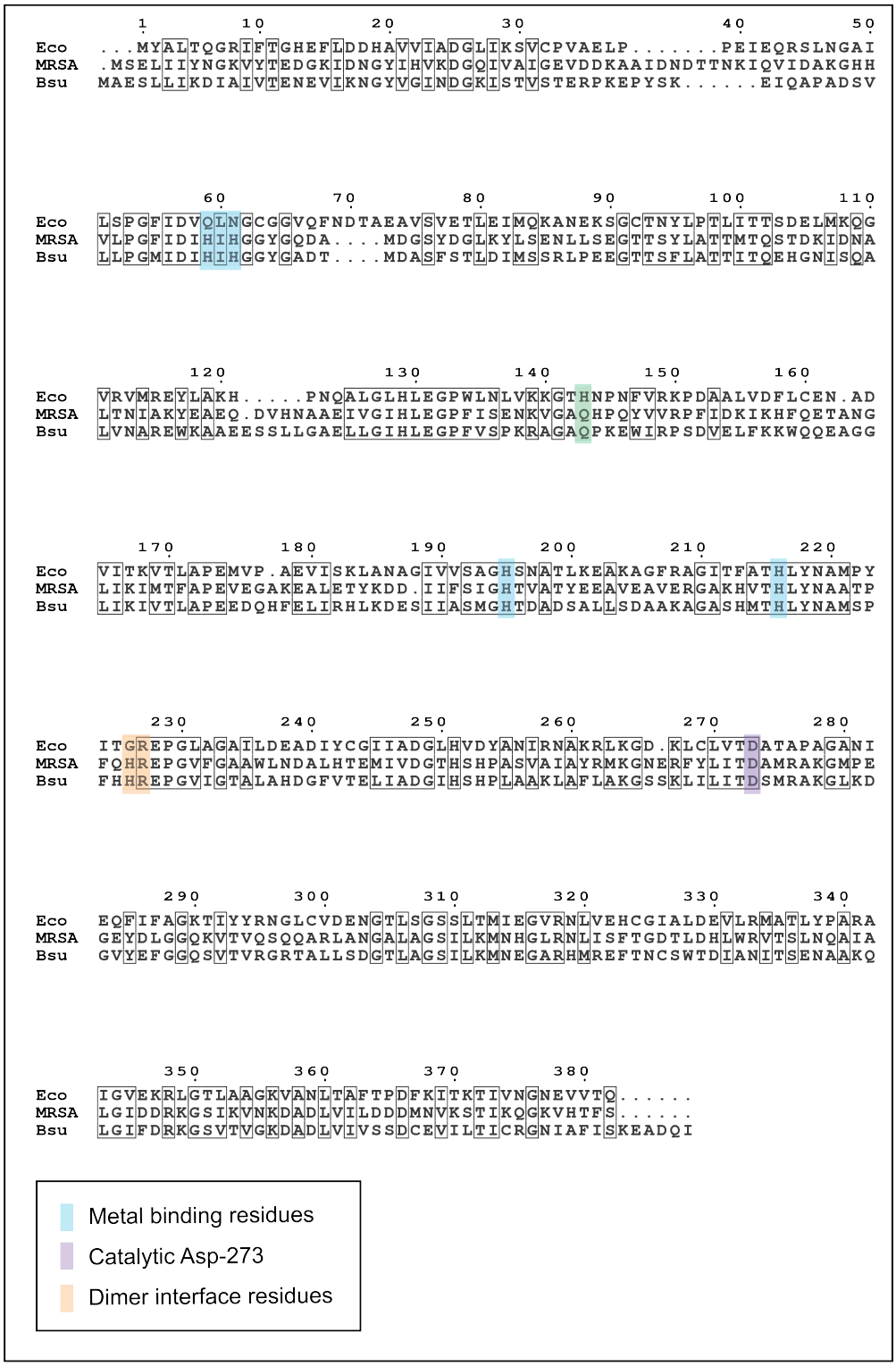

Figure 4. USA300 NagA sequence alignment with *E. coli* NagA (Eco) and *B. subtilis* NagA (Bsu). The MRSA-USA300 NagA amino acid sequence was aligned with the *E. coli* (29% sequence identity) and *B. subtilis* (46% sequence identity)

1.6 NagB: structure and catalytic chemistry

NagB is a member of the hydrolase superfamily, belonging to the aldose-ketose isomerase class of proteins (Oliva, 1995). Crystal structures have been reported from a number of bacterial species, including *E. coli* (Oliva, 1995)*, B. subtilis* (Vincent, Davies, & Brannigan, 2005)*, Streptococcus mutans* (Liu, Li, Liang, Li, & Su, 2008)*, Vibrio cholerae* (PDB: 4R7T) *and Borrelia burgdorferi* (PDB: 3HN6). Described as a having a three-layer α/β/α sandwich fold, the body of the enzyme encloses the active site in what resembles a Rossman-like fold (Vincent et al., 2005). NagB is also distinguished by a highly flexible helix-loop that is suggested to form an 'active-site lid' in the *E. coli*, *B. subtilis and S. mutans* enzymes.

In the forward direction, NagB catalyses the deamination of glucosamine-6-phosphate with water to produce fructose-6-phosphate and an ammonium ion (Fig 3.). The catalytic mechanism for this reaction is suggested to resemble other aldose-ketose isomerases, starting with a binding and ring-opening step, proton abstraction from C2 to form a *cis*-enediol intermediate, followed by a ring closing step and dissociation. In the NagB mechanism the substrate is suggested to form a *cis*-enolate-ammonium intermediate, followed by the formation of an unstable carbinol-ammonium intermediate which decomposes to give the products (Oliva, 1995). In *S. mutans* the ring opening step is thought to be achieved by an Asn-His-Glu catalytic triad that carries out proton transfer from the O1 to the O5 of the sugar ring, breaking the O5-C1 bond. This catalytic triad is conserved in the MRSA sequence, as shown in blue (Fig 5.). The asparagine and glutamic acid residues help polarise the histidine residue, encouraging proton abstraction from O1. The consensus in the literature is that the main residue involved in catalysing the removal of the amino group is an aspartic acid residue (Asp-72 in *E. coli*), which abstracts a proton from C2. This residue is conserved in the MRSA NagB sequence (Fig 5.).

The quaternary structure of NagB varies greatly between species. In *E. coli*, NagB forms a homohexamer, in a trimer of dimers arrangement. In the gram-positive *Streptococcus mutans* and *B. subtilis* species of bacteria, NagB is a monomeric enzyme (Liu et al., 2008; Vincent et al., 2005) It has been proposed that throughout evolution NagB in Gram-positive

bacteria have diverged into a monomeric family, simultaneously losing the allosteric regulation seen in the *E. coli* enzymes (Vincent et al., 2005). This is supported by the sequence alignment shown in Fig. 5.

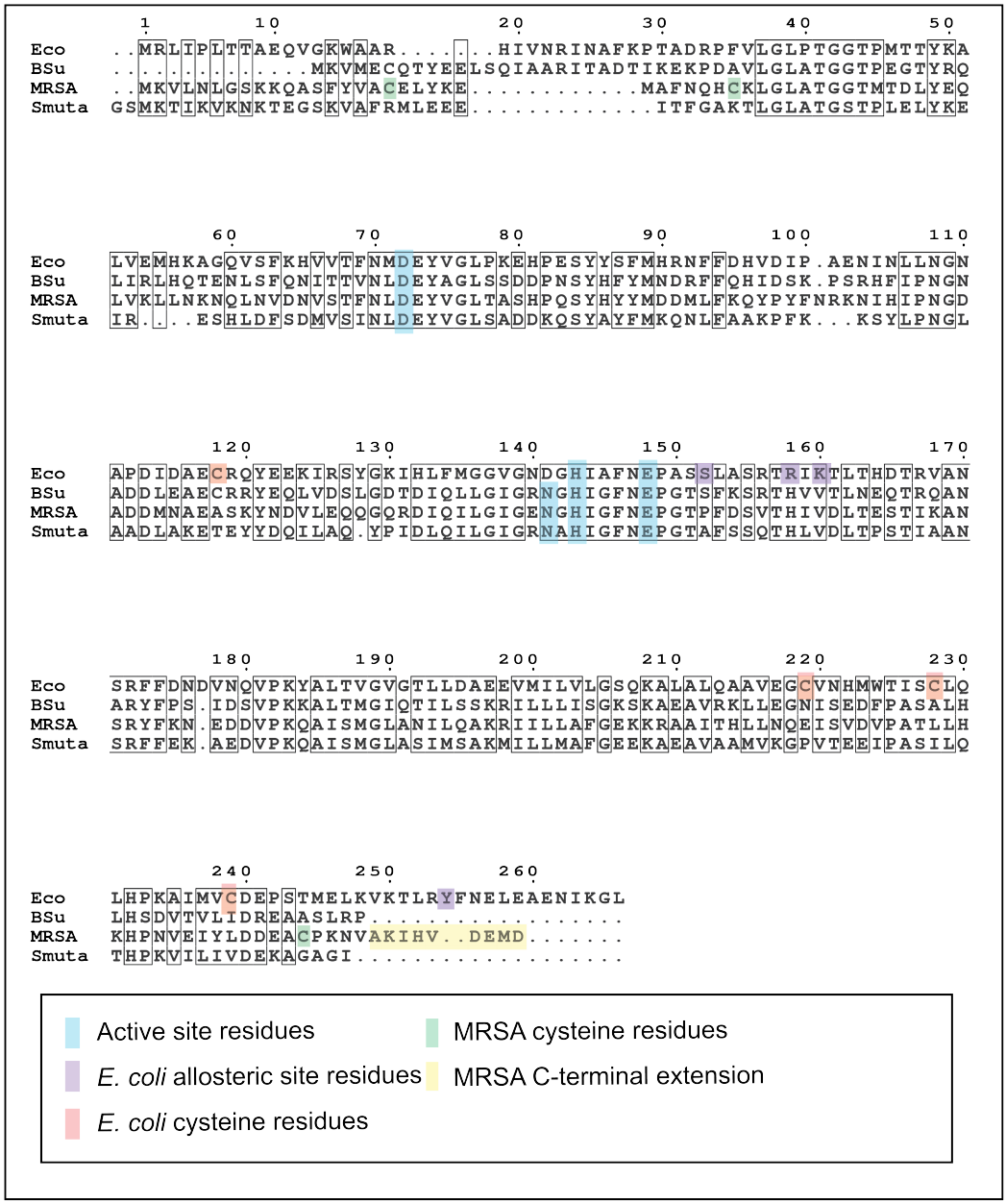

Figure 5. Sequence alignment of MRSA NagB. Highlighted are key residues implicated in catalysis and allostery. MRSA NagB was aligned to the amino acid sequences of *S. mutans* (45% identity), *B. subtilis* (50% identity) and *E. coli* (33% identity).

1.7 Summary

The uptake and catabolic pathways for amino sugars converge upon NagA and NagB, that in concert with GlmS, control the distribution of amino sugar precursors to major metabolic pathways. Here, a network of pathways that direct metabolites to NagA and NagB have been proposed. In order to coordinate these pathways, nuanced control over the enzymes in these pathways is needed, as seen in other species of bacteria. Described as a 'gateway' controlling cell wall synthesis in *S. aureus*, little is known about the structure, function or regulation of enzymes in this gateway. The structure and catalytic abilities of NagA and NagB have been characterised in a number of species, but to date, there have neem no structural or kinetic characterisation of NagA and NagB reported from *S. aureus*. This thesis presents the first biophysical and kinetic analysis of NagA and NagB from a clinically relevant strain of MRSA.

Chapter Two:

MRSA NagA is a dimer that displays complex kinetic behaviour in solution

Overview

This chapter demonstrates the first purification and crystallisation of methicillin-resistant *Staphylococcus aureus* *N*-acetylglucosamine-6-phosphate deacetylase (NagA) and a subsequent biophysical characterisation using a number of techniques. Size exclusion chromatography coupled with multi-angle light scattering (SEC-MALS) and analytical ultracentrifugation (AUC) experiments were conducted to assess the quaternary structure of NagA in solution. Small-angle X-ray scattering (SAXS) experiments were conducted to provide shape information and build *ab initio* models depicting the 3-D structure of MRSA NagA in solution.

Secondly, this chapter presents a kinetic analysis of MRSA NagA. This constitutes the first characterisation of the reaction kinetics of a *N*-acetylglucosamine deacetylase enzyme from a gram-positive species of bacteria. Given the divergence of active site architecture and metal ligation schemes between species (Hall, Brown, et al., 2007), these experiments provide a basis for further investigation of the catalytic mechanism, and provide insight into how NagA functions in MRSA.

Results and Discussion

2.1 Purification and crystallisation of MRSA NagA

MRSA NagA was purified to near homogeneity *via* a three-step purification procedure, as described in Chapter 6. The purification protocol was based on that used for other enzymes characterised from MRSA (North et al., 2014). Purification was analysed using sodium-dodecyl sulfate polyacrylamide gel electrophoresis (SDS-PAGE), as shown in Fig 6. Bands corresponding to the theoretical monomer weight of NagA (43.2 kDa) are visible. Biophysical characterisation was performed using protein of a purity the same or as close as possible to that seen in lane six, where the purity was estimated to be upward of 95%.

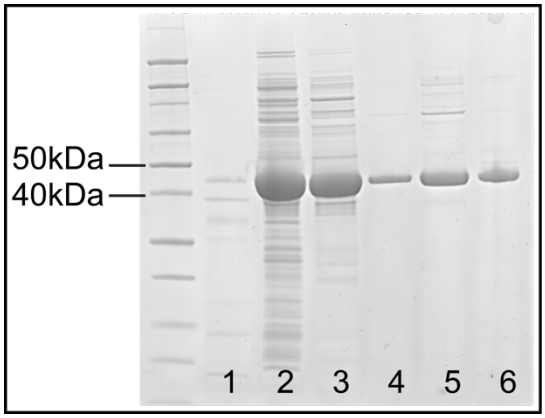

Figure 6. SDS-PAGE gel from MRSA NagA purification. **(1)** Insoluble material after lysis, **(2)** clarified lysate, **(3)** eluate from AEC, **(4)** eluate from HIC, **(5)** eluate from left-shoulder of size-exclusion peak, **(6)** eluate from right shoulder of size-exclusion peak.

Crystallisation trials were routinely performed using pure preparations of MRSA NagA, as described in Chapter 6. Fig. 7. shows crystals grown in 2 M calcium acetate, 10% polyethylene glycol 20,000 and 10% polyethylene glycol 550 monomethyl ether. These crystals appeared to be particularly sensitive to temperature and movement, and would show significant rounding at the edges over time.

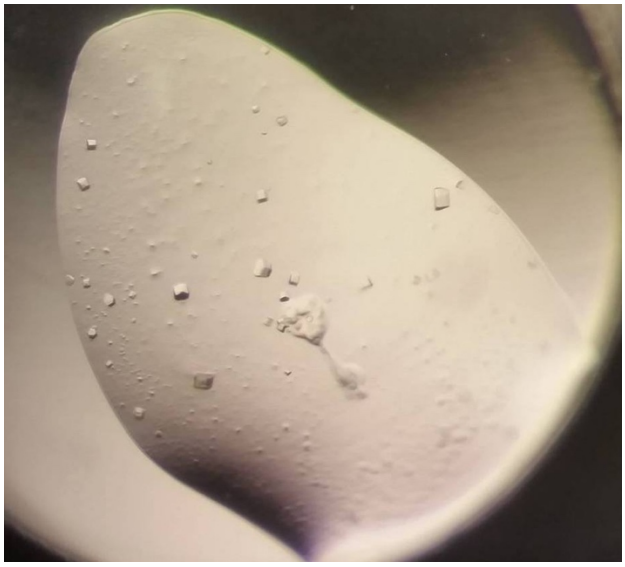

Figure 7. MRSA NagA protein crystals.

Preliminary diffraction experiments at the Australian Synchrotron showed these crystals diffracted very poorly, but did not appear to show the characteristic diffraction pattern of salt crystals. Optimisation of this condition was attempted by adding the substrate, *N*-acetylglucosamine-6-phosphate (GlcNAc-6P) to the condition, and systematically varying the relative concentrations the polyethylene glycol precipitants, and the pH of the buffer. This condition requires further optimisation to improve diffraction.

2.2 MRSA NagA forms a dimer as determined by size-exclusion chromatography coupled multi-angle light scattering

Size-exclusion chromatography coupled with multi-angle light scattering (SEC-MALS) was used to characterise a pure sample of MRSA NagA at a concentration of 2.1 mg/mL, as detailed in Chapter 6. The data shown here (Fig. 8.) indicate that NagA is primarily a dimer in solution, with a retention volume of 12.62 mL and a predicted molecular mass of 88.6 kDa, consistent with the theoretical mass of 86.3 kDa. Integration of the small peak at ~11 mL gave mass estimates of approximately 220 kDa. This is inconsistent with a higher oligomer of NagA, and is more likely to be a contaminating protein or aggregate.

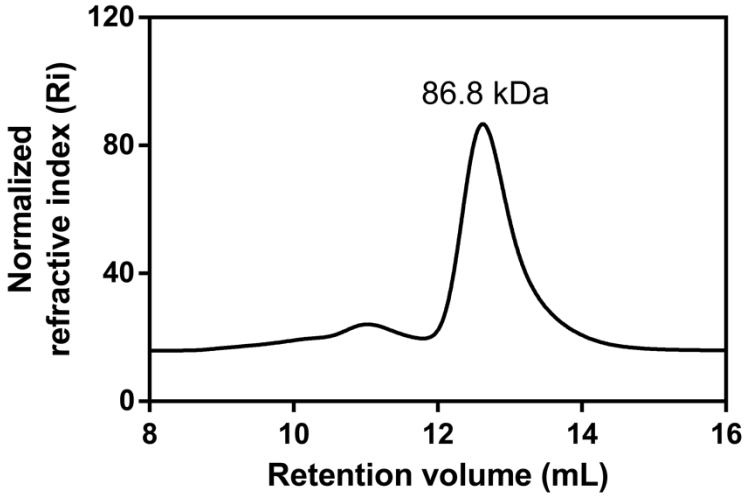

Figure 8. NagA SEC-MALS data: normalised refractive index versus retention volume.

2.3 MRSA NagA forms a dimer as determined by analytical ultracentrifugation

Sedimentation velocity (SV) analytical ultracentrifugation (AUC) experiments demonstrate that NagA exists predominantly as a dimer in solution. This experiment was performed using NagA at a concentration of 0.3 mg/mL. The data collected were fitted to a continuous sedimentation coefficient distribution model, [c(*s*)]. This gave a single symmetrical peak with a sedimentation coefficient of 4.99 S (Fig. 9. A), and a frictional ratio (f/f_0) of 1.34. This f/f_0 is a value that is a property of the hydrodynamic shape of a protein in solution (an f/f_0 of 1 represents a sphere), and here this value supports a moderately extended shape, such as an ellipsoid .

This [c(*s*)] distribution was transformed to give a mass distribution [c(*M*)] model with an apparent molecular mass of 86.7 kDa, which is again consistent with a theoretical dimer mass of 86.3 kDa. The absorbance at 280 nm versus the radial position shows a single sedimenting boundary, which is consistent with the presence of a single species (Fig.9. B). The residuals (magnitudes of deviation of the model from the data) are low in value and randomly distributed, indicating the c(*s*) model adequately describes the raw sedimentation data (Fig. 9. C).

A

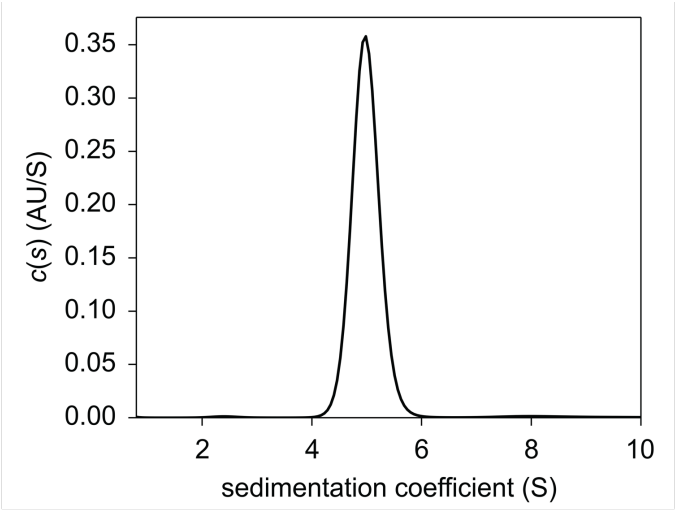

B

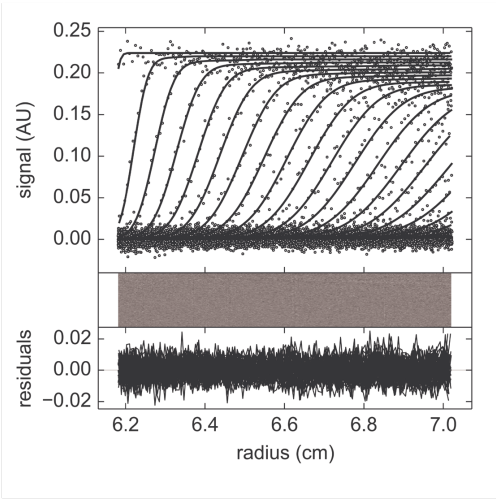

C

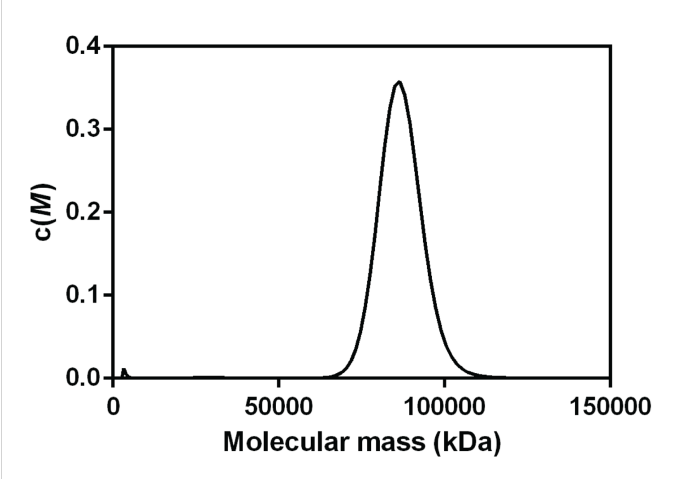

Figure 9. NagA AUC data **(A)** The *c*(*s*) distribution as a function of the sedimentation coefficient **(B)** Top: Absorbance at 280 nm plotted as function of the radial position, Bottom: The residuals of the fit **(C)** c(*M*) model plotted as a function of molecular mass (kDa).

2.4 NagA shape determination and ab initio *modelling from small-angle X-ray scattering experiments*

Small angle X-ray scattering (SAXS) experiments again confirm the dimeric quaternary structure MRSA NagA, and provide details about the size and shape of the protein in solution. The data displayed was collected from protein at a starting concentration of 6 mg/mL prior to dilution during the experiment. The scattering profile of NagA shows a relatively low signal to noise ratio, with the data does become noisy at high scattering angles, particularly around 0.6 $Å^{-1}$ (Fig. 10 A). The Guinier plot (Fig. 10. B) of the NagA scattering data shows linearity at low *q* angles, indicating scattering was not adversely effected by either aggregation or interparticle interference. This linearity is required for further data analysis to be useful. When high concentrations of protein (~13 mg/mL) were trialled, the data collected showed severe interparticle interference for both proteins, which could not be analysed accurately.

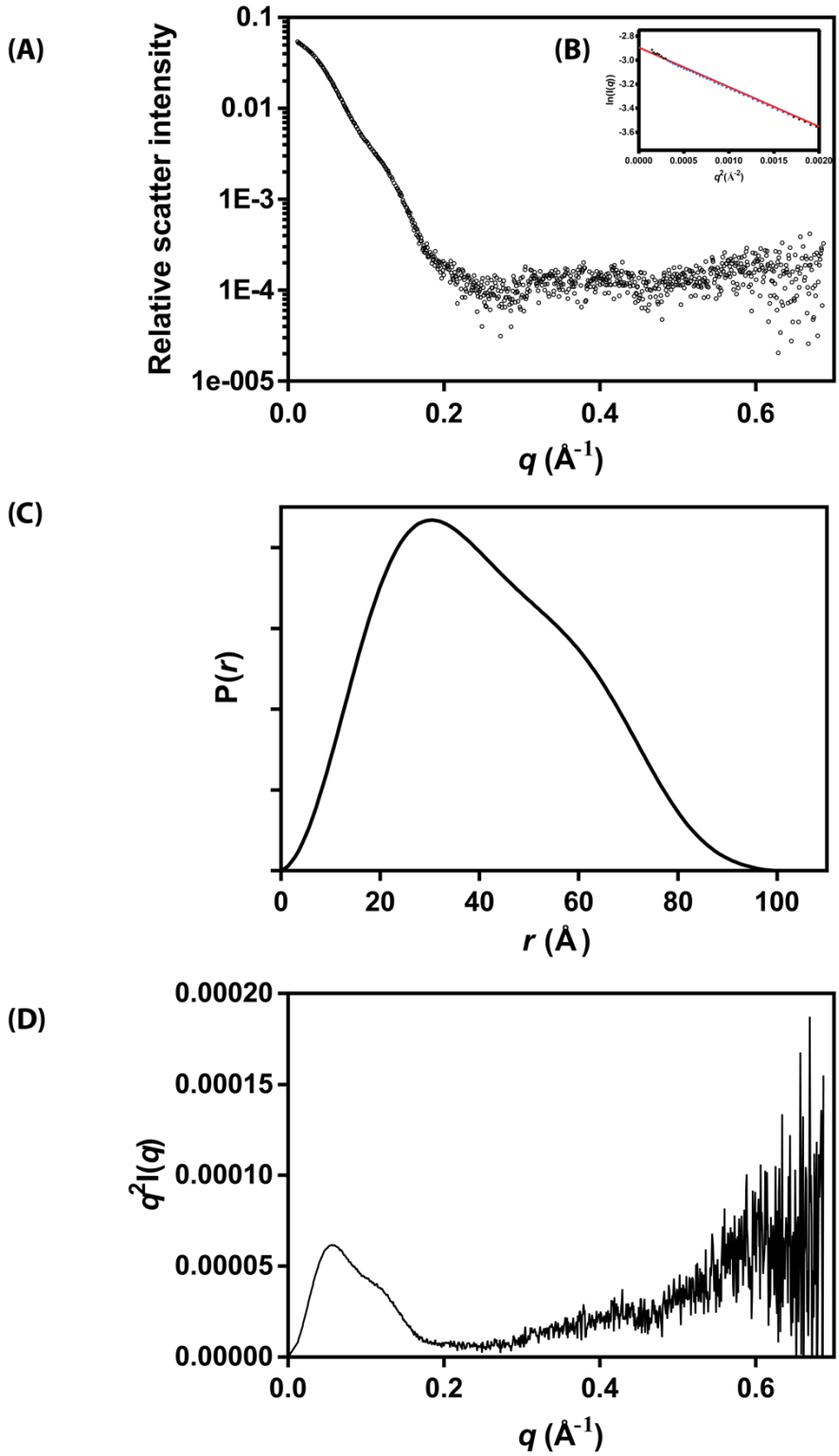

Figure 10. MRSA NagA SAXS data. **(A)** Solvent-subtracted scattering profile showing relative scatter intensity versus scattering vector. **(B)** Guinier plot. **(C)** Distance distribution plot. **(D)** Kratky plot.

Guinier analysis using *PRIMUS* (Petoukhov et al., 2012) gave a forward scattering value (I_0) of 0.068, and a radius of gyration R_g of 31.58 Å. This is in agreement with the R_g calculated using *GNOM*. The maximum distance (D_{max}) of NagA was calculated here as 100.9 Å using *GNOM*.

The distance distribution *P(r)* plot shows the distribution of distances between any two points in the protein scattering envelope, and here shows a slight positive skew toward long distances. This could be interpreted as the shape of the scattering particle being closer to an ellipsoid than a sphere, and supports the observation of an extended shape in AUC. The Kratky plot (Fig. 10. D) demonstrates the protein is folded in solution, and indicates a degree of flexibility in the protein, as shown by the upward trend at higher *q* angles. This SAXS data was also analysed using *SAXS MoW2* (Fischer, de Oliveira Neto, Napolitano, Polikarpov, & Craievich, 2009) which gave a predicted molecular mass of 86.3 kDa. This is in line with the aforementioned molecular mass estimates.

CRYSOL (Petoukhov et al., 2012) was used to calculate a theoretical solution scattering curve for the *B. subtilis* dimer and fit it to the solution scattering profile of NagA. As shown in Fig. 11., this theoretical scattering curve fitted the data well, giving a reduced X^2 value of 0.21. This suggests that the *B. subtilis* structure is a good approximation for the shape and structure of the MRSA NagA dimer in solution.

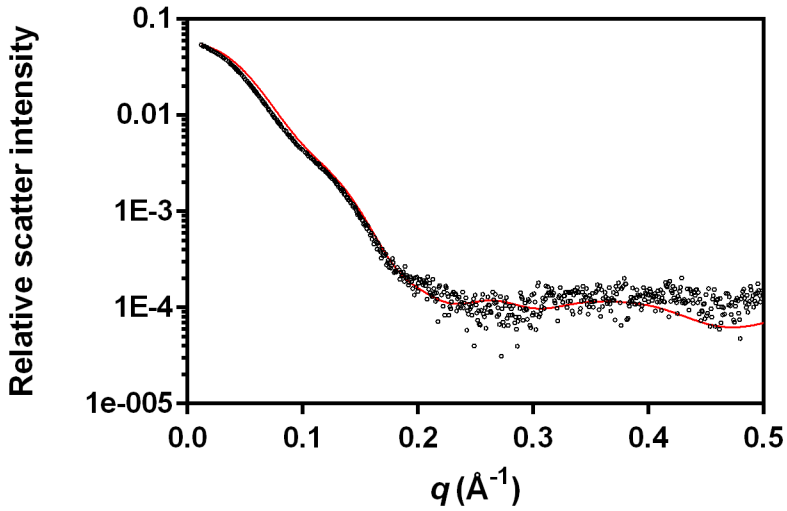

Figure 11. NagA scattering profile (black) fitted with the theoretical scattering curve of *B. subtilis* NagA (red).

An *ab initio* model of MRSA NagA was generated using GASBOR with enforced P2 symmetry. The model gave a X^2 against the raw data of 1.0, and 0.3 against data corrected by the program. As shown in Fig. 12. B., the crystal structure of *B. subtilis* NagA aligns well with the *ab initio* model, supporting the idea that the structure of *B. subtilis* NagA is a good approximation for what MRSA NagA may look like in solution.

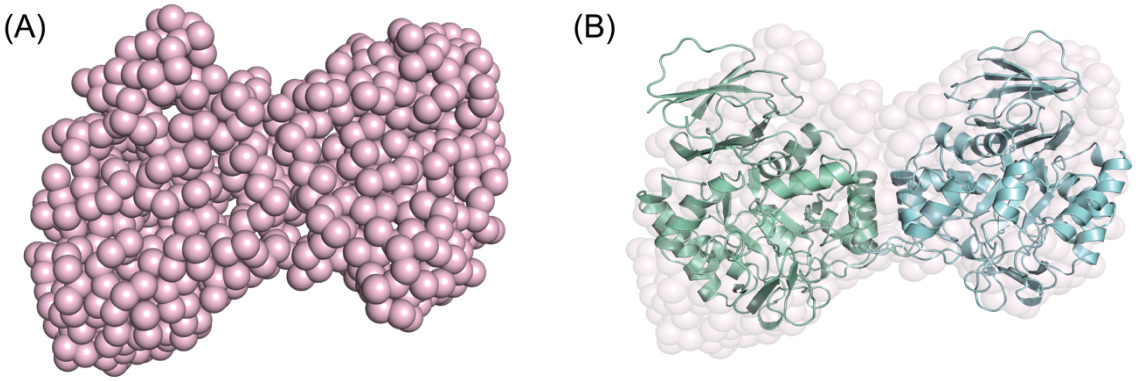

Figure 12. (A) *Ab initio* model of MRSA NagA, generated using *GASBOR.* **(B)** *Ab initio* model aligned with *B. subtilis* NagA dimer. This alignment was generated by *SUPCOMB.*

2.5 MRSA NagA may show a hysteretic response to changes in substrate concentration

MRSA NagA kinetics were performed using a direct continuous assay, as described in Chapter 6, where the rate of GlcNAc-6-P deacetylation catalysed by NagA was measured directly at 215 nm (Souza, 1997). After initial purifications and kinetic analyses of MRSA NagA, it was found that the measured rate could be enhanced through the addition of $ZnCl_2$ to the growth media during the overexpression of NagA. Presumably, this is due to insufficient metal cofactor availability during growth, or loss of the metal cofactor during protein purification. Supplementation of the growth media with 1 mM $ZnCl_2$, as seen in other NagA expression conditions (Hall, Brown, et al., 2007), greatly reduced this effect, and thus the kinetics presented here are from these enzyme preparations only.

A significant lag phase was observed at higher substrate concentrations, as shown in Fig. 7. This lag phase was observed consistently with different batches of enzymes. This was initially

interpreted as substrate inhibition, although it is expected that if this is the case the initial velocity would be reduced, rather displaying a lag. As shown in Fig. 13., this lag became increasingly prominent at substrate concentrations greater than 0.5 mM. At 1 mM this lag increased to around 60 seconds, which is significant in the time course of the reaction. Several factors such as cold inactivation of the enzyme, temperature equilibration of the reaction mix and buffer pH were investigated as potential causes of this unusual phenomenon, yet controlling for any of these factors did not affect the observed lag. Loss of a metal cofactor was also considered as a potential cause, yet addition of $ZnCl_2$ to the reaction mix also had no effect on the observed lag.

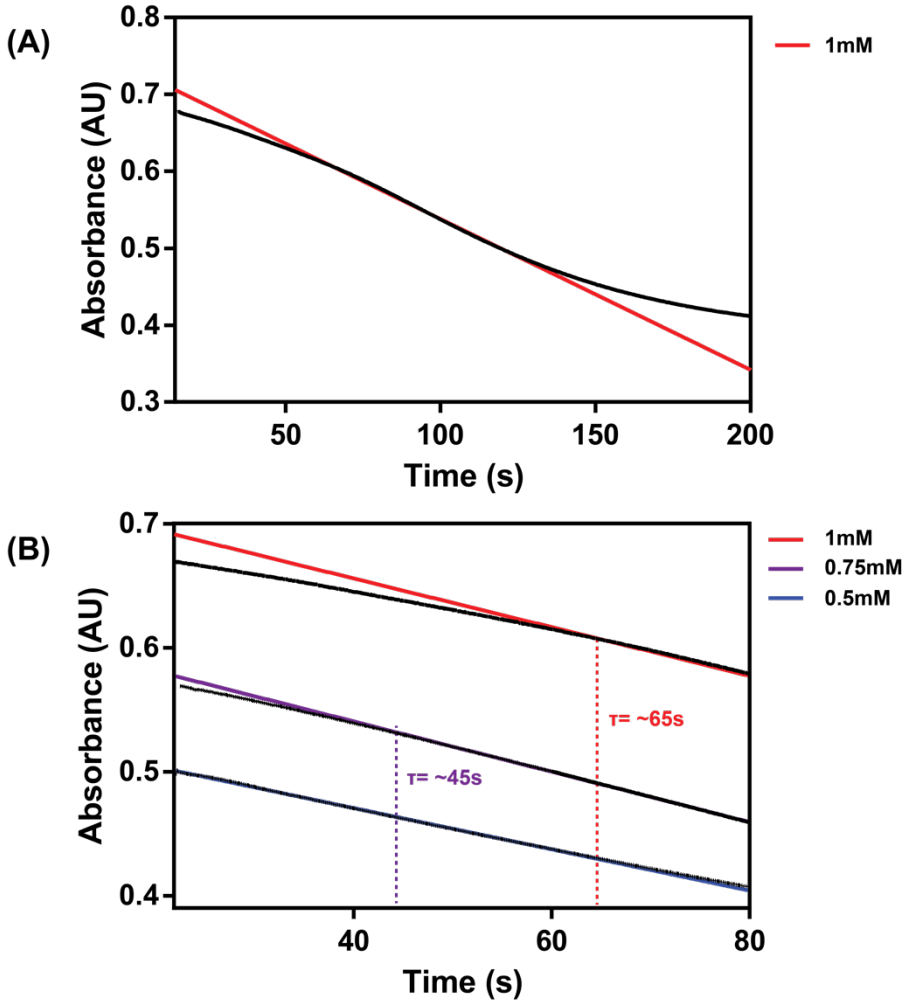

Figure 13 (A) Absorbance versus time shows lag period at 1mM substrate (GlcNAc-6-P). Coloured lines show linear regression to the steepest Δ absorbance (fastest reaction velocity). (B) Absorbance versus time shows increase of lag period as GlcNAc-6-P increases in concentration

One potential explanation is that MRSA NagA is displaying hysteretic kinetic behaviour. A hysteretic enzyme is defined as an enzyme that responds slowly to a rapid change in ligand, substrate or concentrations. Slow conformational isomerisations are thought to be responsible for many hysteretic responses, where conformers have different kinetic properties. Another mechanism that explains hysteretic behaviour is ligand-induced oligomerisation (Frieden, 1979).

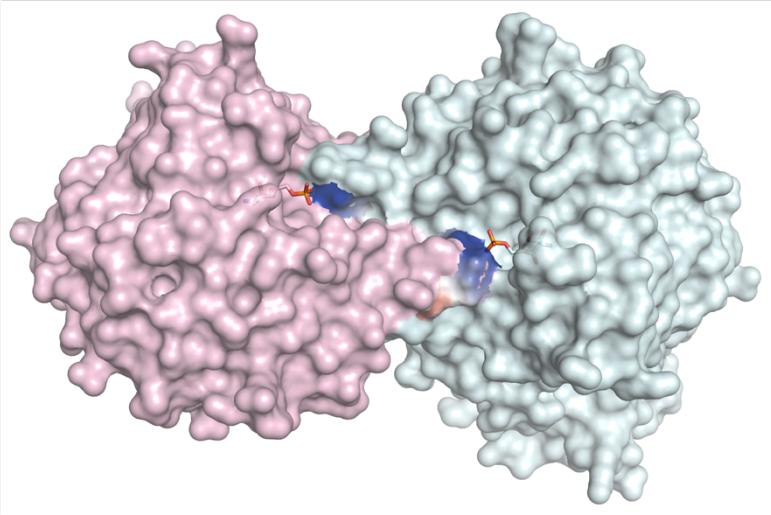

Figure 14. Surface model of the *B. subtilis* NagA dimer (top view). The phosphate moiety of the product GlcN-6-P (shown in orange) is seen protruding out from the surface of one monomer, and interacting with positively charged residues (dark blue) of the other monomer. Figure adapted from (Vincent et al., 2004)

Considering the way in which *B. subtilis* NagA dimerises, hysteresis as a response to ligand-induced oligomerisation is plausible for MRSA NagA. As shown in Fig. 14, two residues, His-233 and Arg-234 from the $\beta_6\alpha_6$ loop of each monomer protrude into the active site of the opposite monomer, where they are suggested to stabilise the phosphate moiety of the substrate (Vincent et al., 2004). The involvement of each monomer in binding substrate gives rise to the potential for ligand-induced dimerization, and for the monomer and the dimer to each have different kinetic properties.

As demonstrated earlier, MRSA NagA exists as a dimer in solution which resembles the *B. subtilis* arrangement. This was established by measurements made in the low μM concentration range, however at the low nM concentrations of enzyme used in this assay it

is possible that a proportion of the enzyme exists in a monomeric conformation, and that this population may well have different binding or catalytic properties to the dimer, that in turn could lead to a lag period.

These types of hysteretic response are thought to play a role in regulation of metabolism– a lag could cause a time-dependent buffering of metabolites, which may well be important in pathways which utilise common intermediates, or where there are multiple branch points (Frieden, 1979). As already mentioned, NagA catalyses the formation of a product that is a common intermediate, and is either fed into peptidoglycan biosynthesis or glycolysis, and this lag phase could be part of a mechanism that buffers against rapid flux in the multiple pathways feeding into NagA. However, the relevance of a lag phase in *vivo* is uncertain, as intracellular GlcNAc-6-P concentrations are unknown. It is conceivable that rapid increases in GlcNAc-6-P to the concentrations used in this assay could occur through the combined actions of the peptidoglycan recycling, sialic acid and *N*-acetylglucosamine uptake pathways. In this case, a hysteretic MRSA NagA could function to buffer GlcN-6-P production, which may in turn be important for pathway timing or optimal function of enzymes in the downstream pathways.

2.6 MRSA NagA kinetic behaviour can be described using the Michaelis Menten model

The aforementioned lag was ignored when fitting the classic Michaelis-Menten kinetic model using *GraphPad*.

$$\upsilon = \frac{V_{max}[S]}{Km + [S]}$$

Equation 1: Michaelis-Menten model

Fitting this model to the data using nonlinear regression gave parameters as follows: a maximum velocity (V_{max}) of 480 $\pm$ 9 μmol · min^{-1} · mg^{-1}, a Michaelis-Menten constant of (K_m) 0.16 $\pm$ 0.01 mM, and a catalytic turnover number (k_{cat}) of 320 $\pm$ 6 s^{-1}. The fit shown has an R^2 value of 0.96, indicating the model fits the data well (Fig. 15). These parameters are within the same order of magnitude as those reported in the literature: for *E. coli* NagA, the K_m is 0.08 $\pm$ 0.1 mM and the k_{cat} 102 $\pm$ 2 s^{-1} (Hall, Xiang, Xu, & Raushel, 2007).

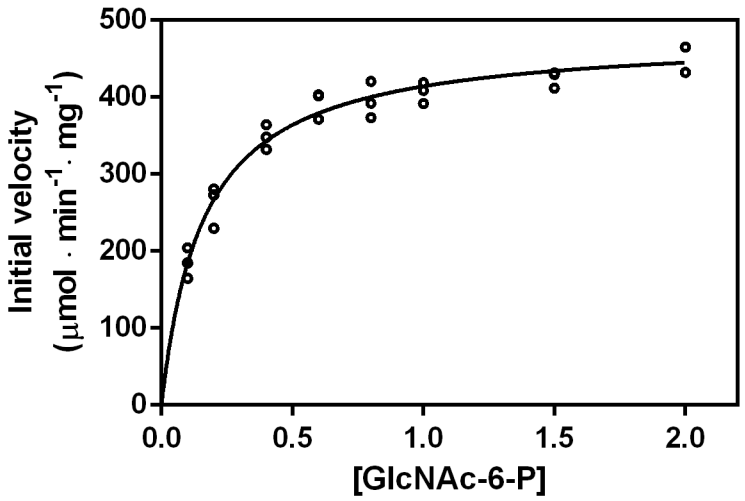

Figure 15. MRSA NagA initial velocity versus substrate (GlcNAc-6-P) concentration (mM) data.

These kinetic parameters are the first reported from gram-positive bacteria, and based on predictions made by sequence alignment, may be the first reported for a NagA enzyme with a binuclear metal centre. This is of interest as these proteins have diverged greatly in terms of active site architecture and mechanisms, and it is still unclear whether or not there are differences in the catalytic power between the mononuclear and divalent metal systems. Further structural information is needed to determine how MRSA NagA binds and uses metal ions in catalysis. In comparing MRSA NagA catalytic activity to that reported for *E. coli* NagA, it is noted that the MRSA enzyme has a three-fold higher k_{cat} than that of *E. coli* NagA, which may hint at the differences in catalytic power between the mononuclear and binuclear NagA enzymes. However, this value is dependent on the accuracy of enzyme concentration measurement, which can be variable in the literature.

Conclusions

Biophysical experiments show that MRSA NagA exists predominantly as a dimer in solution. As shown in Table 1, the techniques used here all support this finding, giving molecular mass estimates close to the theoretical mass calculated from the amino acid sequence.

Technique	Theoretical monomer	Theoretical dimer	SLS	AUC	SAXS
Predicted mass (kDa)	43.1595	86.319	86.3	86.7	86.3

Table 1: Predicted molecular mass of MRSA NagA as estimated by a number of biophysical techniques.

Taken together, the SEC-MALS and AUC data show that MRSA NagA forms a relatively tight dimer in solution. The SAXS data supports the hypothesis that the MRSA NagA dimer resembles that of the *B. subtilis* enzyme in solution. This is further strengthened by the conservation of key residues shown to be involved in dimerisation. The SAXS analysis performed here has provided structural parameters for MRSA NagA in solution, such as estimates of the maximum interatomic distance across the enzyme, that in the absence of X-ray crystallographic data, provide some insight into the structure and shape of MRSA NagA.

The kinetics of MRSA NagA show an unusual response to high substrate concentrations, which is proposed here to be a hysteretic property of the enzyme that may have relevance *in vivo*. Here, this property is related to a potential ligand-induced mechanism of dimerisation observed in the *B. subtilis* enzyme. This slow response to a rapid change in substrate concentration may have utility when placed in the context of the proposed utilisation of

amino sugars in MRSA (Chapter 1), where a number of different pathways can direct GlcN-6-P to MRSA NagA, and may be able to greatly increase GlcN-6-P concentrations within MRSA. A slow catalytic response to this could therefore be a buffering mechanism against rapid flux through this pathway, or part of a metabolic timing mechanism.

Chapter Three:

MRSA NagB adopts a novel oligomeric state in solution

Overview

This chapter reports the first purification and crystallisation of methicillin-resistant *Staphylococcus aureus* glucosamine-6-phosphate deaminase (NagB), and the biophysical characterisation of this enzyme to probe its properties. The quaternary structure of NagB is of interest here given the reported divergence of NagB in species of gram-positive bacteria to a monomeric enzyme, as opposed to the allosterically regulated hexamer seen in gram-negative bacteria. The first kinetic analysis of NagB is also presented here. Together these data will underpin future research, such as mutagenic experiments, to understand the catalytic and possible regulation of this enzyme. Finally, this chapter presents the possibility of a protein-protein interaction between NagA and NagB.

Results and Discussion

3.1 Purification and crystallisation of MRSA NagB

As shown by sodium dodecyl sulfate polyacrylamide gel electrophoresis (SDS-PAGE) in Fig. 1A., MRSA NagB was purified to near homogeneity *via* the same three-step purification process as MRSA NagA. Bands are visible corresponding to the theoretical monomer weight of NagB (28.2 kDa). Biophysical characterisation was performed using protein of a purity represented in lane five (Fig. 16.A), which was visually estimated by eye to be upward of 95%.

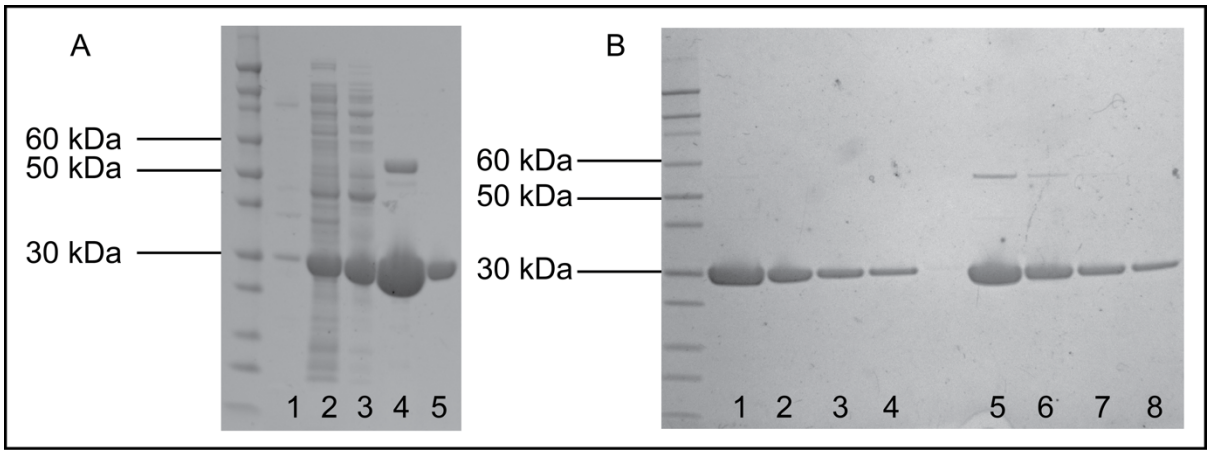

Figure 16. (A) SDS-PAGE gel from MRSA NagB Purification. **(1)** insoluble material after lysis, (2) clarified lysate, (3) eluate from AEC, (4) eluate from HIC, (5) eluate from SEC. **(B)** LDS-PAGE gel of purified NagB in the presence of 1mM TCEP (5,6,7,8), and absence of TCEP (1,2,3,4). 1; 1mg/mL, 2; 0.5mg/mL, 3; 0.25 mg/mL and 4; 0.1 mg /mL.

Under reducing conditions with 1 mM tris(2-carboxyethyl)phosphine (TCEP), the purified protein shows that one band is visible, corresponding to the theoretical monomeric molecular weight of 28 kDa. Without TCEP, the same sample shows a second band between 50 and 60 kDa, as seen in lanes 5 and 6 (Fig. 1B), corresponding to the theoretical molecular mass of an MRSA NagB dimer. This result suggests NagB dimer formation is somehow dependent on non-reducing conditions, and it is hypothesised here that NagB dimerisation may therefore involve formation of a disulfide bond. Coincidently, an SDS-PAGE and kinetic analysis reported in the literature has found that in *Escherichia coli* NagB can form a disulfide-linked dimer within its

overall hexameric organization, formed by a cysteine residue at position 219 (Altamirano, 1993).

Cys-219 is not conserved in MRSA NagB as shown in the NagB sequence alignment (Chapter 1). However, there are three cysteine residues in the sequence that could be involved in disulfide bond formation. A good candidate for this is Cys-238, which is located in near the C-terminus of the NagB sequence. This cysteine is not found in monomeric NagB enzymes, and the equivalent residue in the high identity *B. subtilis* sequence, Ala-236, is shown to be solvent accessible at the C-terminus. Additionally, the C-terminus of MRSA is conspicuously elongated compared to the gram-positive monomeric enzymes. Further investigation and structural data are needed to test these hypotheses.

Crystallisation trials were routinely performed using pure preparations of MRSA NagA, as described in Chapter 6. A condition was identified for the crystallization of MRSA NagB using the PACT HT-9 commercial crystal screen (Molecular Dimensions): 0.2 M sodium citrate tribasic dehydrate and 20% w/v polyethylene glycol 3350. This condition was optimized in-house, which led to growth of the crystals shown in Fig. 17. A. X-ray diffraction experiments performed at the Australian Synchrotron using these crystals gave diffraction to a maximum resolution of 8-9 Å, which is too low to build accurate protein structural models from the electron density. Optimisation of this condition was then performed at the C3 Collaborative Crystallisation Center, as described in Chapter 6, which yielded a number of crystals of different morphologies as depicted by Fig.17. B-D. However, these crystals were either fragile or temperature sensitive, and were disrupted upon transport to the Australian Synchrotron. This reported crystallisation is promising, and this condition should be further optimised in future research.

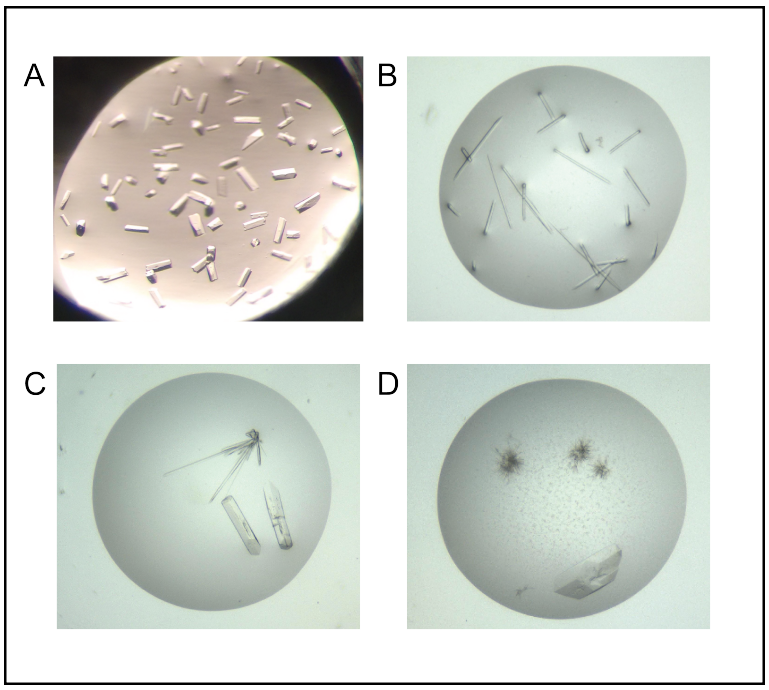

Figure 17. MRSA NagB crystals **(A)** Crystals grown in-house **(B-D)** Different crystal morphologies grown in optimised conditions

3.2 MRSA NagB forms a dimer as determined by size-exclusion chromatography multi-angle light scattering

Size-exclusion coupled with multi-angle light scattering (SEC-MALS) was used to assess the heterogeneity and quaternary structure of MRSA NagB at a concentration of 2.1 mg/mL. The data shown here (Fig. 18.) indicates that NagB is primarily a dimer in solution, with a retention volume of 13.39 mL, and a predicted molecular mass of 55.3 kDa. This is consistent with the theoretical dimer mass of 56.9 kDa. The slightly asymmetric peak may indicate that a small proportion of this sample is in a monomer-dimer equilibrium.

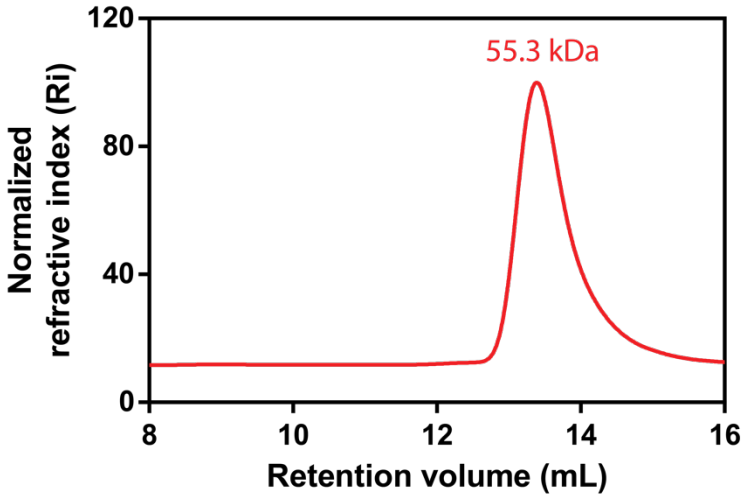

Figure 18. MRSA NagB SEC-MALS: normalized refractive index versus retention volume.

3.3 MRSA NagB forms a dimer as determined by analytical ultracentrifugation

Sedimentation velocity (SV) analytical ultracentrifugation (AUC) experiments support the hypothesis that MRSA NagB is mainly a dimer in solution. This experiment was performed using NagB at a concentration of 0.3 mg/mL. The data were fitted to a continuous sedimentation coefficient distribution model, [c(*s*)], which shows the sample is monodisperse (Fig. 19. A) Integrating the single symmetrical peak gives a sedimentation coefficient of 3.75 S. The frictional ratio coefficient (f/f_0) of 1.46 indicates that the protein has an extended shape in solution (an f/f_0 of 1 represents a sphere). Fitting this data to the continuous mass distribution [c(*M*)] model gave an apparent molecular mass of 61.8 kDa, which is close to the theoretical dimer mass of 56.9 kDa (Fig. 19. C).

A small peak is observed with a sedimentation coefficient of 2 S, which gave an apparent molecular mass of 25.1 kDa, although this peak is responsible for only 1% of the total signal. The existence of this peak supports the observation of a slight monomer-equilibrium in SEC-MALS experiments, although it is clear that at the concentrations studied here, NagB is predominantly dimeric.

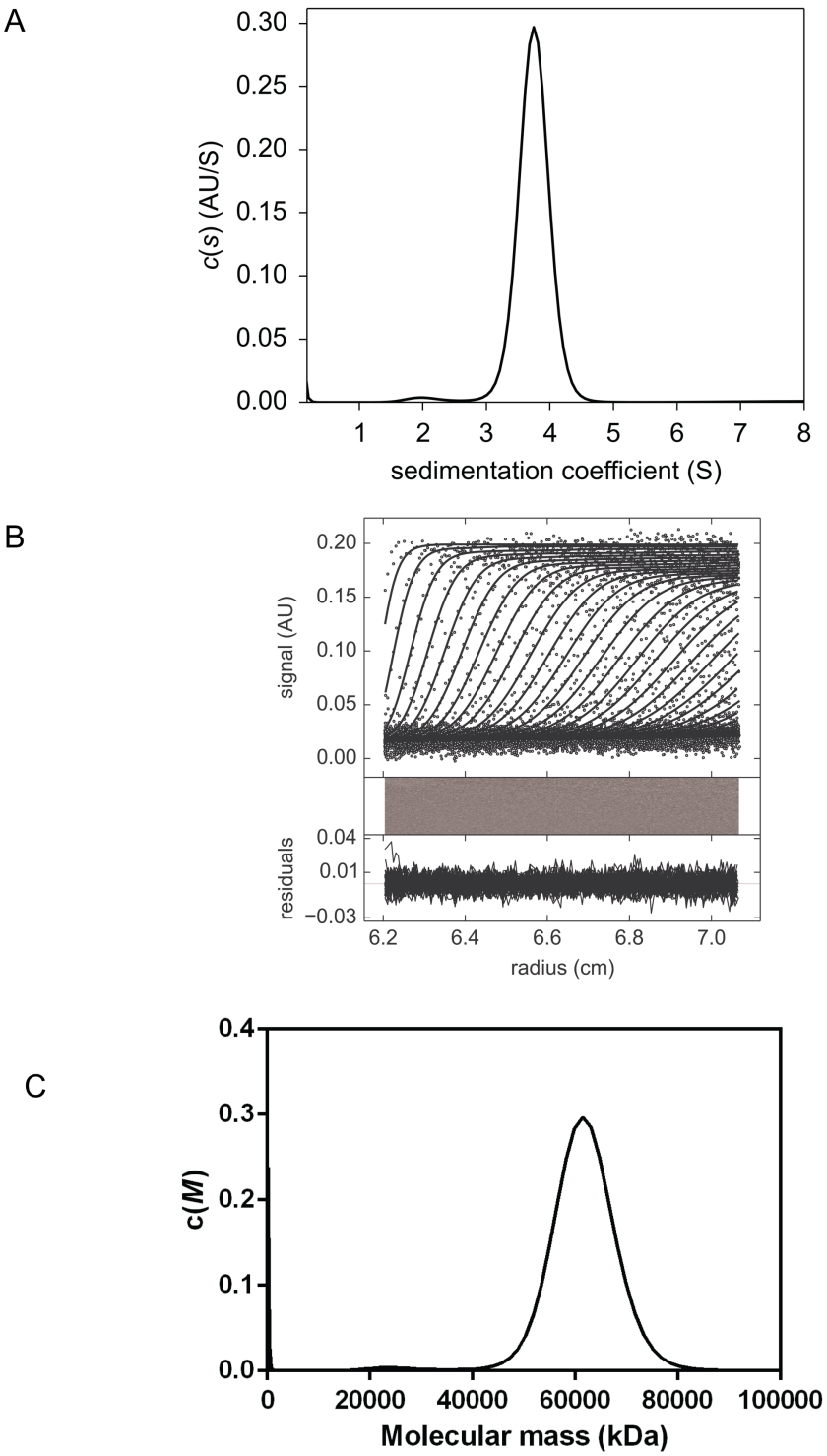

Figure 19. MRSA NagB AUC data. **(A)**. *c(s)* distribution as a function of the sedimentation coefficient. **(B)**. Top: Absorbance at 280 nm plotted as function of the radial position, shows a single sedimenting boundary. Bottom: The residuals of the fit, which are randomly distributed. (**C)**. *c(M)* model plotted as a function of molecular mass (kDa).

3.4 NagB shape determination and ab initio *modelling from small-angle X-ray scattering experiments*

Small-angle X-ray scattering (SAXS) was performed using a 6 mg/mL sample of MRSA NagB to gauge the shape of the molecule in solution. Guinier analysis of this SAXS data shows an upturn at low *q* angles (Fig. 21. B) indicating aggregation in the sample. However, a linear region could still be defined, and the data points outside of this region were excluded in this analysis. *PRIMUS* (Petoukhov et al., 2012) calculated a forward scattering value (I_0) of 0.068, and a radius of gyration R_g of 27.25 Å which is in agreement with the R_g calculated using *GNOM*. The maximum interatomic distance (D_{max}) of NagA was calculated from the as 101 Å using *GNOM*.

The distance distribution *P(r)* plot shows a relatively symmetrical peak, with a very slight shift toward longer distances. This could be interpreted as the shape of the scattering particle being closer to an ellipsoid than a sphere, and supports the observation of an extended shape in AUC. The Kratky plot (Fig. 21D) shows the protein is folded in solution, and indicates a degree of flexibility in the protein, as shown by the upward trend at higher *q* angles. This SAXS data was also analysed using SAXS MoW2 (Fischer et al., 2009) which gave a predicted molecular mass of 59.8 kDa. This is in line with the aforementioned molecular mass estimates.

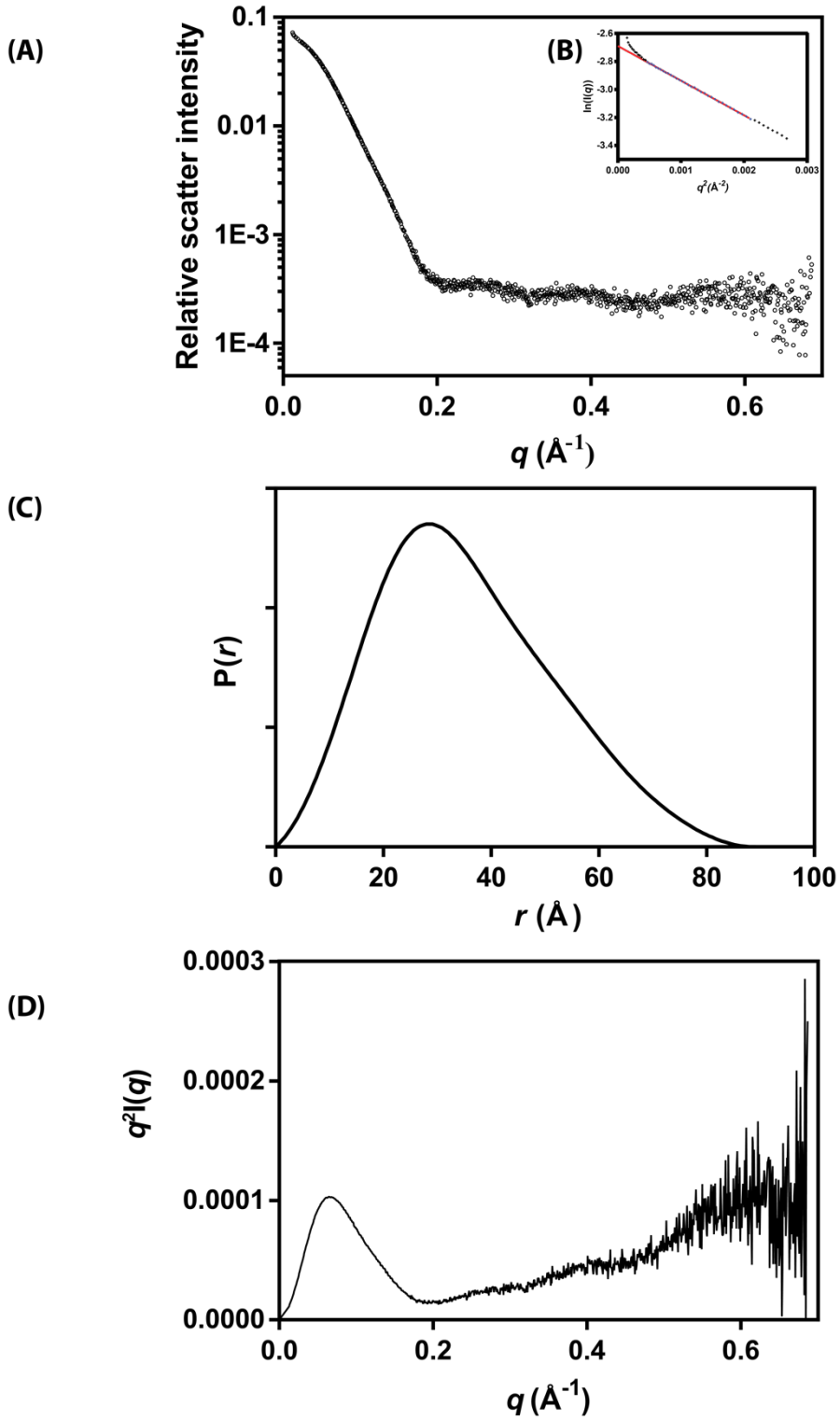

Figure 3: MRSA NagB SAXS data. **A)** Solvent-subtracted scattering profile showing relative scatter intensity versus scattering vector. **(B)** Guinier plot. **(C)** Distance distribution plot **(D)** Kratky plot.

GASBOR (Petoukhov et al., 2012) was used to generate an *ab initio* model of MRSA NagB, using enforced P2 symmetry (Fig. 22.). This symmetry is not necessarily the biological organization of NagB, but is likely given the dimeric nature of the protein, and gave a good fit to the raw scattering data with a X^2 value of 2.0 against the raw data, and 0.79 against data corrected by *GASBOR*. Currently this model is only useful for providing an indication of the potential shape of MRSA NagB, and could not be fitted accurately with any of the available NagB crystal structures.

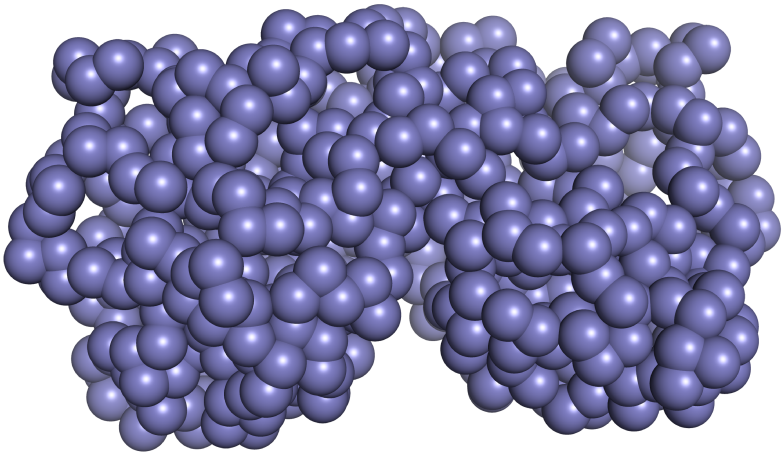

Figure 22. *Ab initio* model of MRSA NagB generated using *GASBOR.*

3.5 MRSA NagB kinetics reveal a pattern of substrate inhibition

The kinetics of MRSA NagB were performed using a coupled-coupled assay as described by (Vincent et al., 2005) and elaborated in Chapter Six. The initial velocities observed using this assay are displayed in Fig. 23. A clear reduction in the initial velocity of the reaction is seen with increasing concentration of substrate, glucosamine-6-phosphate (GlcN-6-P). These data were fitted using the classic substrate inhibition model using *GraphPad* software

$$v = \frac{V_{max}[S]}{K_m + [S] + \frac{[S]}{K_i}}$$

Equation 2: Substrate inhibition model

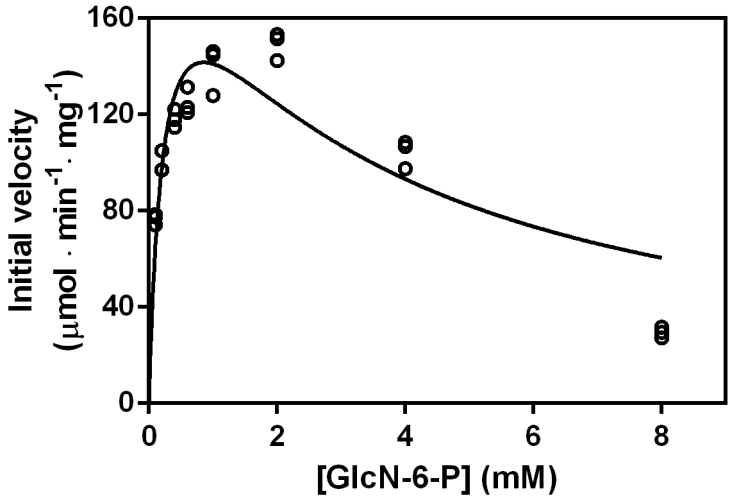

Figure 4. MRSA NagA initial velocity versus substrate (GlcNAc-6-P) concentration data.

The fit shown has an R^2 value of 0.78, which was the best fit achieved using common models of kinetic behaviour. Fitting the model (Eq. 2) using nonlinear regression gave parameters as follows: a maximum velocity (V_{max}) of 222 $\pm$ 33 μmol · min^{-1} · mg^{-1}, a Michaelis-Menten constant (K_m) for GlcN-6-P 0.24 $\pm$0.08 mM, an inhibitory constant K_i of 3 ± 1 and a catalytic turnover (k_{cat}) of 176 $\pm$ 16. s^{-1}.

	***B. subtilis* NagB**	***S. mutans* NagB**	**MRSA NagB**
K_m (mM)	0.13 ± 0.02 mM	0.21 ± 0.03	0.24 ± 0.08
K_{cat} (s^{-1})	28 ± 6.0	34.1 ±4.0	175.6 ±16.5

Table 2. Kinetic parameters of gram-positive NagB enzymes compared with those reported here (Liu et al., 2008; Vincent et al., 2005)

Compared to values reported in the literature for NagB from gram-positive bacteria, MRSA

NagB has a similar for K_m for GlcNAc-6-P but a much higher k_{cat} (Liu et al., 2008; Vincent et al., 2005), as shown in Table 1. These reported values all use the assay reported by (Vincent et al., 2005), at the same starting protein concentration. This pattern could possibly be explained by the novel dimeric organization of MRSA NagB, which could possess different kinetic capabilities than the monomeric NagB enzymes.

Notably, no rate increase was observed when GlcNAc-6-P (the allosteric activator for *E.coli* NagB) was added to the assay mixture, or when GlcNAc-6-P was incubated with NagB prior to adding it to the assay. This lack of allostery has also been observed in the monomeric *S. mutans* and *B. subtilis* NagB enzymes, and this finding supports the hypothesis that throughout evolution gram-positive NagB has lost the property of allosteric regulation (Vincent et al., 2005).

The biological relevance of substrate inhibition here is unclear. Liu et al (2008) posit that the the lower activity of Gram-positive NagB compared to Gram-negative NagB may have evolved in response to the higher requirement for GlcN-6-P to be directed into the peptidoglycan biosynthesis pathway. It is possible that during peptidoglycan biosynthesis via GlmS where GlcN-6-P concentrations are high, that substrate inhibition of NagB, alongside low catalytic activity serves to prevent conversion of GlcN-6-P back to Fru-6-P.

3.6 NagA and NagB may have a protein-protein interaction

The potential of a protein-protein interaction between NagA and NagB is also investigated here. Protein interactions are thought to be commonplace in most organisms and play an important role in metabolic pathways, where they can confer efficiency through allow channelling of substrates from enzyme to enzyme, without releasing substrate into the bulk solvent. Additionally these interactions can also affect the activities of enzymes, and contribute to the regulation of pathways in general .

A transient protein-protein interaction between NagA and NagB is plausible, given that they catalyse sequential steps in a pathway, and because they are often co-expressed. The need

for regulation or control over these enzymes also makes the idea of a protein-protein interaction an interesting concept to investigate, as a number of different transient interactions could conceivably modulate both enzyme and pathway activity here.

The hypothesis that NagA and NagB can interact has been briefly addressed in the literature– this has been tested *in vitro* with *B.* subtilis NagA and NagB, where no protein-protein interaction was detected, although the authors do not present any data or methodology (Vincent et al., 2005).

Here, a sedimentation velocity experiment was performed to test for a possible interaction, under the premise transient complex formation in a mixture of NagA and NagB would have different sedimentation properties in comparison to the proteins individually. As shown in Fig. 8A, a mixture of NagA and NagB at a 1:1 ratio (final concentration= 0.3 mg/mL) , as shown in red, shows a slight peak broadening to the right, extending from a value of 6 S to 8 S. This may be taken as evidence of a population of a larger species in solution, but further testing is needed to to confirm this.

SV experiments at a range of protein concentration, as well as in the presence of each substrate should be conducted. One limitation of this experiment is that the buffer conditions do not resemble the physiological conditions inside the cell, or the extremely crowded environment of a cell, where it is suggested that specific protein-protein interactions are more frequent than in *in vitro* experiments given the excluded volume phenomenon (Kuznetsova, Turoverov, & Uversky, 2014). These conditions could be better modelled using a macromolecular crowding agent, such as dextran or polyethyleneglycol, during an AUC experiment.

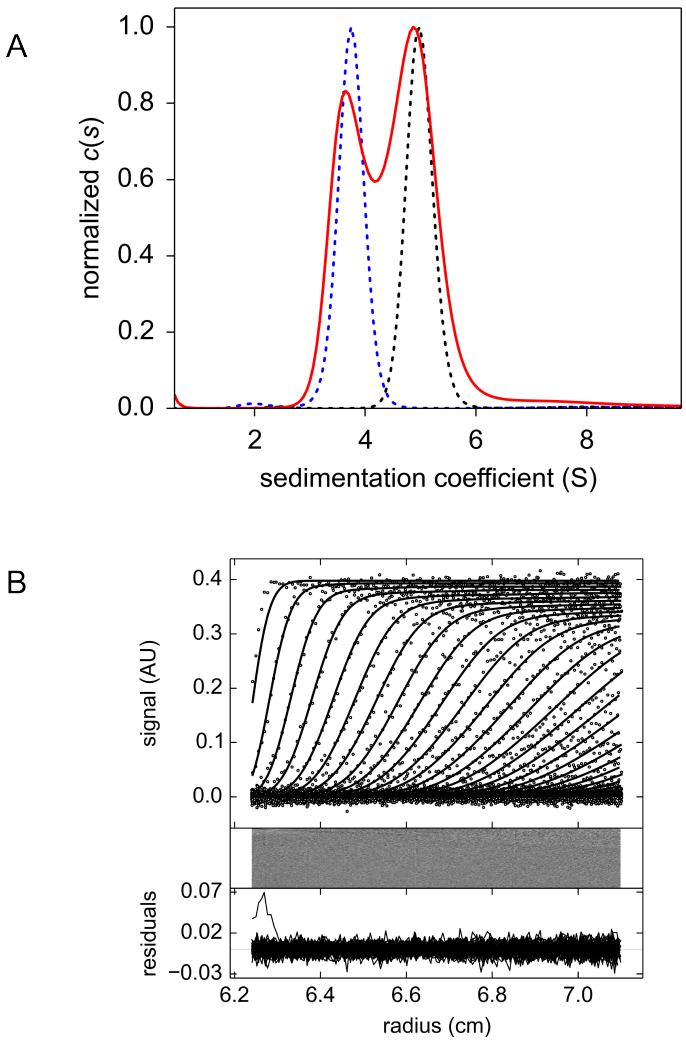

Figure 24 (A) Normalized *c(s)* distribution plotted as a function of the sedimentation coefficient. The red line shows the sedimentation of a mixture of MRSA NagA and NagB, with both proteins at a final concentration of 0.3 mg/mL. The black dotted line shows the separate NagA and NagB sedimentation *c(s)* distributions shown earlier in this thesis.

Conclusions

This chapter presents the first structural and kinetic characterisation of NagB from *Staphylococcus aureus.* The biophysical data shown here demonstrate that MRSA NagB is predominantly a dimer in solution. As shown in Table 2, each technique gives similar molecular mass estimates for NagB.

	Theoretical monomer	**Theoretical dimer**	**SLS**	**AUC**	**SAXS**
Predicted mass (kDa)	28.5	57	55.3	61.9	59.8

Table 3: Predicted molecular mass of MRSA NagB, as estimated by a number of biophysical techniques.

The finding that MRSA NagB is a dimer in solution is an unexpected result, given the quaternary structures for gram-positive bacteria reported in the literature, as depicted in Fig. 8. SDS-PAGE analysis in reducing and non-reducing conditions suggest that this dimer could be held together by a disulfide bond, although this requires further validation. This novel quaternary structure may have implications for the structure, function and regulation of these enzymes– it is suggested here that the MRSA NagA dimer may have different catalytic capabilities in comparison to the monomeric gram-positive enzymes.

Kinetics experiments show a clear pattern of substrate inhibition. The relevance of this is uncertain *in vivo*, but it is speculated here that this inhibition may be useful during peptidoglycan biosynthesis, to avoid the futile cycling of glucosamine-6-phosphate between NagB and GlmS. MRSA NagB also appears to be demonstrate greater catalytic activity compared to other gram-positive bacteria, which could be a property of this novel dimeric organization. Finally, a protein-protein interaction between NagA and NagB is proposed, with preliminary AUC data suggesting this hypothesis needs to be further tested.

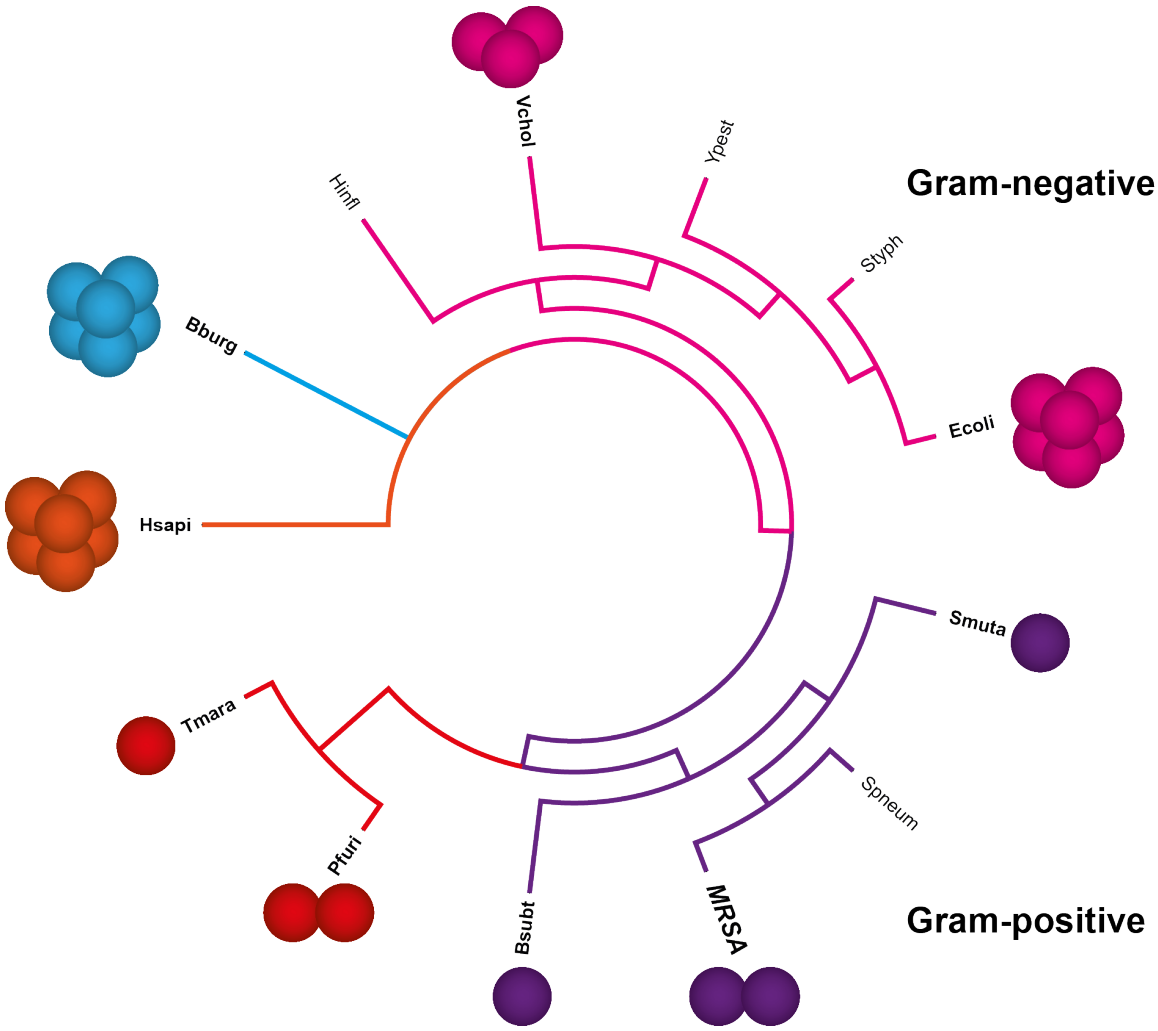

Figure 25. Phylogenetic tree based on amino acid sequence alignment demonstrating the variation in oligomeric state of NagB enzymes. Each coloured spheres represents a protein subunit, and hence the overall oligomeric state. Although not immediately evident in this diagram, the primary sequence of MRSA is closer in identity to the *H. sapiens* primary sequence, demonstrating the great divergence in primary sequence of these enzymes. This tree was generated as described in Chapter 5. Tmara; *Thematoga maratima,* Pfuri; *Pyrococcus furiosus*; Bsubt; *Bacillus subtilis*, MRSA Spneum; *Streptococcus pneumoniae*, Smuta; *Streptococcus mutans*, Ecoli; *Escherichia coli*, Styph; *Salmonella typhimurium* Ypest; *Yersinia pestis*, Vchol; *Vibrio cholerae*, Hinfl; *Haemophilus influenzae*, Bburg; *Borrelia burgdorferi* Hsapi; *Homo sapiens*.

Chapter Four:

Conclusions and future research

This thesis uses a combination of structural biology and enzymology to explore two enzymes, *N*-acetylglucosamine-6-phosphate deacetylase (NagA) and glucosamine-6-phosphate deaminase (NagB), that are involved in amino sugar utilisation in a methicillin-resistant strain of *Staphylococcus aureus* (MRSA). It is suggested here that these enzymes may be novel antibiotic targets, based on their ability to distribute host-derived nutrients into major metabolic pathways— peptidoglycan biosynthesis and glycolysis. The research conducted in this thesis is the first structural and kinetic characterisation of these enzymes from *S. aureus*.

I have developed a purification protocol and discovered conditions that led to crystallisation of both MRSA NagA and NagB, a significant advance towards understanding the structure of these enzymes. It is anticipated that these conditions can be further trialled and optimised to give better X-ray diffraction, from which atomic-resolution models can be built. These models will be required to accurately describe MRSA NagA and NagB structure and function. Crystal structures of these enzymes are also required to inform targeted inhibitor and drug design.

Biophysical experiments revealed that MRSA NagA to be dimeric in solution, and that the *Bacillus subtilis* enzyme appears to be a good approximation for how MRSA NagA might dimerise. Kinetic analyses of MRSA NagA have have revealed an unusual lag period at high substrate concentrations. I put forward here that NagA is demonstrating hysteretic kinetic behaviour, a mechanism of metabolic regulation that buffers against high flux in the pathways that converge on NagA. I propose that kinetic hysteresis is caused by substrate-induced oligomerisation—in this case, forming a dimer in the presence of *N*-acetylglucosamine-6-phosphate. Fluorescence-detection analytical ultracentrifugation experiments should be considered in the future to test this hypothesis. Nevertheless, ignoring the lag period gave typical Michaelis-Menten like kinetic behaviour for MRSA NagA.

An important finding is that MRSA NagB adopts a dimeric quaternary structure in solution– the monomeric state observed in other gram-positive species were until now regarded as representative of the quaternary structure of this enzyme in all gram positive species. It is hypothesised here that this novel oligomeric state may afford MRSA NagB different functional characteristics to both the monomeric, and hexameric forms of NagB. Further research is required to determine the significance of this oligomeric state. Kinetic analyses of MRSA NagB have shown a clear pattern of substrate inhibition. It is also observed that MRSA NagB appears to have a higher catalytic efficiency than the monomeric NagB enzymes, which may be linked to the novel oligomeric state.

The findings in this thesis demonstrate that MRSA NagA and NagB have distinct structural and kinetic properties compared to related enzymes previously characterised in the literature. This warrants further research into these enzymes, to both analyse these properties from an evolutionary standpoint and to better describe how NagA and NagB distribute host-derived amino sugars to different pathways.

Chapter Five:

Experimental

5.1 Experimental reagents

5.1.1 Chemical reagents

N-Acetylglucosamine-6-phosphate and glucosamine-6-phosphate were purchased from Carbosynth. Chemicals used were sourced from Invitrogen and Sigma-Aldrich, unless explicitly stated.

5.1.2 Biological reagents

Phosphoglucoisomerase from *Saccharomyces cerevisiae* and glucose-6-phosphate dehydrogenase from *Leuconostoc mesenteroides* were purchased from Sigma-Aldrich.

5.1.3 General materials

All prepacked chromatography columns were purchased in various sizes from GE Healthcare. BioRad also supplied 96-well plates. Crystallisation screens that were used in-house and solutions used for cryo protection were purchased from Molecular Dimensions. Hampton Research supplied crystallisation plates and cryo loops. All solutions were made with Millipore purified water when required, which is referred to as milliQ water throughout this thesis. Syringe filters were obtained from Millipore. Proteins were concentrated using appropriate molecular weight cut off spin concentrators obtained from Sartorius.

5.2 General methods

5.2.1 pH measurement

The pH of buffer solutions were measured at room temperature using a UB-10 pH/mV meter from Denver Instruments. The instrument was calibrated using pH 4, pH 7 and pH 10 standards (Certipur). Adjustments to pH were made using 1 M or 10 M hydrochloric acid if the pH of the solution required decreasing and 1 M or 10 M sodium hydroxide if the pH of the solution required increasing.

5.2.2 Measurement of protein concentration

Protein concentration was measured using a NanoDrop-1000 spectrophotometer. UV absorbance at 280 nm was monitored and then converted to concentration using the Beer-Lambert law. Protein extinction coefficients were calculated using ExPASy ProtParam (http://web.expasy.org/protparam/).

5.2.3 Antibiotic preparation

Kanamycin was prepared using milliQ water and sterilised using a 0.22 μm syringe filter. The working concentration used in all media was 30 μg/mL.

5.2.4 Luria Bertani medium

Luria Bertani (LB) base was used for all bacterial culturing. LB was prepared by adding 20 g of ready to use powder to 1 L of MilliQ water, and then sterilised by autoclaving.

5.2.5 LB agar

LB base and agar were mixed and prepared in MilliQ water. For every 1 L of LB agar prepared, 20 g of LB base, and 12 g of agar were added to MilliQ water. This was sterilized by autoclaving. Media was supplemented with kanamycin, mixed by gentle swirling and poured into sterile petri dishes in either a laminar flow hood, or close to a flame.

5.3 Bioinformatics

The theoretical molecular weights, extinction coefficients and isoelectric points were computed using the ExPASy ProtParam tool (http://web.expasy.org/protparam/). To search and compare protein and nucleotide sequences, the basic local alignment search tool (*BLAST*) programs *BLASTn* and *BLASTp* were used. Multiple sequence alignments were generated using Clustal Omega (Larkin et al., 2007). Amino acid sequences for Nag homologues were sourced from the NCBI database. Phylemon 2.0 (Sanchez et al., 2011) was used to construct phylogenetic trees using default parameters and bootstrapping and FigTree was used to illustrate generated trees.

5.4 Molecular biology

5.4.1 Cloning

The *nag*A and *nag*B genes were synthesised commercially by Carbosynth and supplied in a pUC57-Kan cloning plasmid. Both genes were cloned into the pET30ΔSE expression vector (Suzuki et al., 2014) by restriction enzyme digestion (*Hin*dIII and *Nde*I) to create pET30ΔSE/*nag*A and pET30ΔSE/*nag*B. The identities of both constructs were confirmed by deoxyribonucleic acid (DNA) sequencing carried out by the University of Otago's genetic analysis service. Approximately 150 ng of purified plasmid DNA and 3.2 pmol T7 promoter primer were supplied in a volume of 5 uL for each sequencing reaction. Data were analysed using the *Geneious* program, and the generated sequences aligned to the expected sequences using *BLASTp.*

5.4.2 Transformation into chemically competent Escherichia coli

The pET30ΔSE/*nagA* and pET30ΔSE/*nagB* constructs were transformed into chemically competent *Escherichia coli* BL21 (DE3) cells according to the manufacturer's protocol (Thermo Fisher Scientific). Approximately 100 ng of each construct was added to 50 μL of competent cells and incubated on ice for 30 minutes. Cells were then heat shocked for 30 seconds at 42 °C and returned to ice for 5 minutes to recover. Super optimal broth with catabolite repression (SOC) media was pre-warmed and 250 μL was added to the cells, followed by an

incubation at 37 °C and 170 revolutions per minute (rpm) for 1 hour. This transformation reaction was then plated out onto LB and agar antibiotic selection plates containing kanamycin and incubated at 37 °C overnight.

5.4.3 Preparation of glycerol stocks

Bacterial strains were stored by culturing 10 mL of transformed *E. coli* cells in LB media containing kanamycin at 37° C and 170 rpm overnight. This was aliquoted into 1.7 mL eppendorf tubes and glycerol was added to a final concentration of 15% (v/v). Tubes were flash cooled in liquid nitrogen and stored at -80 °C.

5.4.4 Large-scale bacterial growth

Starter cultures were prepared by inoculating 10 mL of LB containing kanamycin with a single colony from an antibiotic selection plate. These cultures were grown at 37 °C and 170 rpm overnight. The 10 mL starter culture was then added to 1 L of LB with kanamycin in 5 L baffled Erlenmeyer flasks. These were grown at 37°C and 170 rpm until an optical density at 600 nm (OD_{600}) of 0.55-0.6 was reached. For both NagA and NagB, 4 L of bacterial culture was grown for each purification.

5.4.5 Overexpression

When an OD_{600} of 0.55-0.6 was reached, protein overexpression was initiated by adding isopropyl β-D-1-thiogalactopyranoside (IPTG) to a final concentration of 1 mM in the 1 L flasks. When overexpressing NagA, 1 M $ZnCl_2$ was also added to each flask to maximise metal cofactor binding.

5.4.6 Cell lysis

Cells were pelleted by centrifugation at 10,000 rpm and 4 °C for 15 minutes using a Thermo Sorvall preparative centrifuge. The cell pellets were resuspended in approximately 40 mL of lysis buffer comprised of 20 mM Tris-HCl, pH 8.0 and 0.1mM of the protease inhibitor phenylmethane sulfonyl fluoride (PMSF). Cell lysis was carried out using a Hielschler Ultrasonic processor at 70% amplitude in cycles of 0.5 s on, 0.5 s off for 15 minutes. This step was performed on ice to prevent excessive heating of the sample. Cell debris was then

pelleted by centrifugation using the preparative centrifuge at 15,000 rpm and 4 °C for 15 minutes. The lysate containing the soluble protein was then decanted off and filtered using a 0.22 μm filter.

5.5 Protein purification

5.5.1 General

All chromatography steps were performed using an Åkta HPLC protein purification system at 4 °C, with samples kept on ice between each step to minimise both protein aggregation and degradation by any contaminating proteases. All buffers were prepared fresh, and filtered through a 0.22 μm filter before use. The components of each buffer solution used throughout purification steps are described in Table 1. Both NagA and NagB were purified using the same procedure.

5.5.2 Anion exchange chromatography

Anion exchange chromatography (AEC) was used as the first purification step, where the protein of interest and contaminating proteins were separated based on surface charge. Following cell lysis, the clarified lysate was loaded onto a 20 mL Q sepharose column, containing positively charged resin, pre-equilibrated with five column volumes of buffer A. The column was then washed with 3-5 column volumes of AEC buffer A to wash away any unbound material, until a baseline absorbance at 280 nm was reached. Bound protein was then eluted using a continuous gradient of AEC Buffer B, over 3-4 column volumes. In the first purification, sample corresponding to all 200 nm absorbance peaks were analysed by sodium dodecyl sulfate polyacrylamide gel electrophoresis (SDS-PAGE) to determine where each protein elutes (see Section 6.5.5). Both NagA and NagB eluted at a conductance value of approximately 18-20 mS/cm.

5.5.3 Hydrophobic interaction chromatography

Hydrophobic interaction chromatography (HIC) was used as an intermediate purification step following AEC. Ammonium sulfate was added to the pooled AEC eluent to a final

concentration of 1 M. A 15 mL QFF Phenyl resin column was equilibrated with five column volumes of HIC buffer A prior to sample loading. Sample was then eluted from the column using a continuous gradient of HIC Buffer B, over 3-4 column volumes. Eluted fractions corresponding to 280 nm absorbance peaks were analysed by SDS-PAGE for the protein of interest before being pooled. After the approximate conductance value at which each protein or any major contaminants eluted off the column was determined, isocratic elution was used in subsequent purifications to speed up the elution. NagA bound tightly to the resin and eluted late off the column, at a conductance of approximately 4-5 mS/cm. NagB eluted earlier a broad peak, starting at approximately 80 mS/cm.

5.5.4 Size exclusion chromatography

Size exclusion chromatography (SEC) was used as a final polishing step for the purification of both NagA and NagB proteins. A HiLoad Superdex 200 16/60 120 mL column was used and equilibrated with 4-5 column volumes of SEC Buffer. Eluate from HIC was concentrated to approximately 1% of the column volume using the appropriate molecular weight cut off spin concentrator. Eluted fractions corresponding to 280 nm absorbance peaks were analysed by SDS-PAGE for the protein of interest before being pooled. Following size-exclusion, protein that was not immediately used was flash cooled using liquid nitrogen and stored at -80 °C.

Lysis Buffer	20mM Tris-HCl, 0.1mM PMSF, pH 8.0
AEC Buffer A	20mM Tris-HCl, pH 8.0
AEC Buffer B	20mM Tris-HCl, 1M NaCl, pH 8.0
HIC Buffer A	20mM Tris-HCl, 1M $(NH_4)_2SO_4$ pH 8.0
HIC Buffer B	20mM Tris-HCl, pH 8.0
SEC Buffer	20mM Tris-HCl, pH 8.0

Table 4. Buffers for protein purification and kinetics experiments.

5.5.5 *Sodium dodecyl sulfate polyacrylamide gel electrophoresis*

SDS-PAGE was used to assess the relative purity of protein samples. Novex NuPAGE 4-12% Bis-Tris gels were loaded with 10 uL of sample. The reaction mix was as follows: 10uL sample, 10uL Novex 4 × lithium dodecyl sulfate (LDS) sample buffer, 16uL H_2O and 4 uL of 2mM dithiothreitol (DTT). Sample, LDS sample buffer and H_2O buffer were mixed, then heated at 80 ^{o}C for 15 minutes. After heating, the DTT reducing agent was added. Novex Sharp Pre-stained Protein Standard was also run on the gel so that protein molecular weight could be estimated. The gel was then run for 35 minutes at 135 V. Protein bands were stained using SimplyBlue Coomassie G-250 stain for an hour, and then destained in water overnight. Gels were imaged using a CHEMI GENIUS2 bio-imaging system (Syngene).

5.6 Size-exclusion chromatography coupled with multi-angle light scattering

Size-exclusion chromatography coupled with multi-angle light scattering (SEC-MALS) was carried out using a Viscotek 302-040 Triple Detector GPC/SEX system (ATA Scientific), operated at 28 ^{o}C. Protein sample (100 μL) at 2.1 mg/mL was injected into a 24 mL Superdex 200 10/300 gel filtration column, equilibrated with SEC buffer. Measurements were calibrated against bovine serum albumin standard (BSA) at 4 mg/mL, which was run prior to and after the samples of interest. Baseline, integration limit fitting and mass calculation were all performed using the OmniSEC software.

5.7 Analytical ultracentrifugation

Sedimentation velocity (SV) experiments were performed using an XL-I Analytical Ultracentrifuge (Beckman Coulter). Proteins were centrifuged at 50,000 rpm at 20 °C. Radial absorbance data were collected at 280 nm without averaging for a total of 125 scans. In these experiments, 400 μL of reference and 380 μL of sample solutions were loaded into 12 mm double sector cells with sapphire windows, and then mounted into an An-60 Ti eight-hole

rotor. Solvent viscosity and density, as well as estimates of the partial specific volume of were calculated using the program SEDNTERP (Laue 1992). Sedimentation data were fitted to a continuous size distribution [c(*s*)] model using the program SEDFIT. These data were then fitted to a continuous mass distribution [c(*M*)] in SEDFIT to ascertain the apparent molecular mass of each species observed. GUSSI was used to illustrate the output from SEDFIT.

5.8 Small angle X-ray Scattering

5.8.1 SAXS data collection

Small angle X-ray scattering (SAXS) data were collected at the SAXS/WAXS beamline (Australian Synchrotron) equipped with a Pilatus 1M detector. The wavelength of the X-rays used was 1.0332 Å. For both proteins analysed, 50 μL of sample at 6 mg/ml was run through a Superdex 200 5/150 GL column size-exclusion column, pre-equilibrated with Tris-HCl pH 8.0. Two-dimension intensity plots were radially averaged, normalised to sample transmission, and background subtracted using the Scatterbrain software package (Australian Synchrotron). When a higher concentration of a 13 mg/ml was used the data collected showed severe interparticle interference for both proteins, which could not be analysed accurately.

5.8.2 SAXS data analysis

All SAXS data analyses were performed using the ATSAS software package (version 2.8.0) (Reference). PrimusQT was used to perform the Guinier analyses and the indirect Fourier transform of the data to give the *P*(*r*) distribution. Crysol was used to calculate theoretical scattering from atomic coordinates and compare them to the experimental scattering curves. GASBOR was used to build *ab initio* models of both proteins, and SUPCOMB was used to align crystal structures to the *ab initio* models.

5.9 Kinetics

5.9.1 General

Kinetics experiments were carried out on a Cary 100 Bio UV/Vis spectrophotometer (Agilent Technologies). Enzyme assays were performed in triplicate, and the initial velocity measurements were reproducible to within 10% error. All enzymes and substrates were kept on ice throughout the duration of the assays. Substrates and buffers were prepared on the day of the assay.

5.9.2 NagA direct continuous assay

Kinetic analysis of NagA was performed using a direct continuous spectrophotometric assay, as described by (Souza, 1997). Here, the rate of reaction was measured by following the decrease in ultraviolet (UV) absorbance at 215 nm of the carboxamido group of GlcNAc-6-P, as a function of time. The assay was performed at 30 °C in quartz cuvettes with a path length of 10 mm. The cuvettes were soaked in nitric acid overnight to remove any contaminants that may cause noise in the UV trace. Protein was freshly purified for kinetic analysis and hard-spun at 15,000 rpm and 4 °C for 15 minutes to remove any protein aggregate.

Two controls were performed. Firstly, it was ensured that there was no change in absorbance caused by either enzyme or substrate by themselves. Secondly, it was ensured that the concentration of enzyme used for kinetic analysis was in the linear range. This meant that changing the concentration of enzyme resulted in a proportional increase in rate.

Buffer used in the assay was equilibrated in the spectrophotometer's peltier module for 20 minutes. The pH of the 20 mM Tris-HCl was initially adjusted at room temperature to approximately 0.2 pH units below the desired pH, as the pH of Tris-HCl decreases with increasing temperature. The pH was measured again after equilibration using a micro-pH meter. Enzyme was kept on ice throughout the assay to reduce any decrease in activity or aggregation that might occur. Reaction mixing was performed as quickly as possible using long reach pipette tips. Initial rate data were analysed and fitted using GraphPad Prism software.

5.9.3 NagB coupled-coupled assay

Kinetic analysis of NagB was performed using a coupled-coupled assay, as described by (Vincent et al., 2005). The reaction was observed by measuring the decrease in UV absorbance at 340 nm due to the consumption of reduced nicotinamide adenine dinucleotide phosphate (NADPH), as shown in Fig. 1.

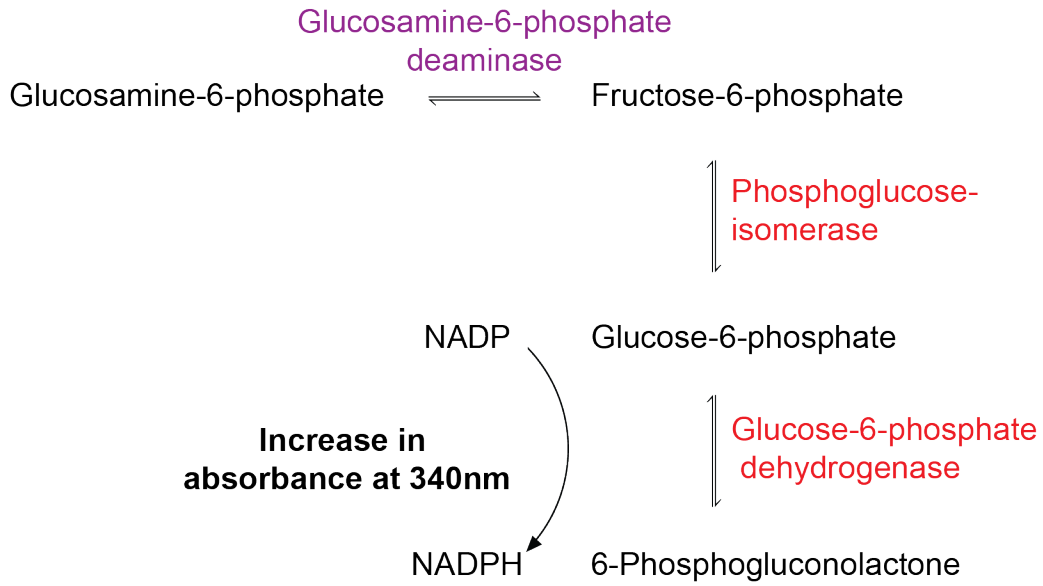

Figure 26. NagB coupled-coupled assay

Again, NagB used in this assay was freshly purified, and hard-spun at 15,000 rpm and 4 °C for 15 minutes to remove any protein aggregate. The reaction was performed in acrylic cuvettes with a 1 mm path length. Reaction mixtures were allowed to equilibrate at 20 °C for 20 minutes in the heat-controlled peltier module. The reaction was performed at this temperature due to the low thermostability of the coupling enzymes. Controls were performed to ensure that both the enzyme concentration was within the linear range, and that each coupling enzyme (shown in red, Fig. 1.) was in excess.

The reaction was initiated by the addition of 20 µL of NagB to give a final concentration of 0.3 µg/mL. Coupling enzyme concentrations were first trialled at 2 µg/mL (PGI) and 3 µg/mL (G6PDH), as reported in the literature, but it was found that these concentrations needed to be increased dramatically to eliminate lag in the initial reaction rate: to 25 µg/mL and 50 ug/mL respectively. Both coupling enzymes were harvested by centrifugation at 10,000 rpm

and 4 ^{o}C, The supernatant was decanted and the resultant enzyme was resuspended in Tris-HCl, pH 8.0. Coupling enzyme concentration was then confirmed spectrophotometrically at 280 nm. Substrate concentration was varied from 0.1 mM to 8 mM. The assay mixture used is as follows: 20 mM Tris-HCl, 5 mM $MgCl_2$, 1 mM NADP+, 25 μg/mL PGI, and 50 μg/mL G6PDH.

5.10 X-ray crystallography

5.10.1 Crystal trials

Crystallisation experiments were performed using freshly purified preparations of protein at at between 10-20 mg/mL. Protein was concentrated using spin concentrators with an appropriate molecular weight cut-off. NagA protein was able to be concentrated upward of 20 mg/ml without aggregation, whereas NagB was prone to aggregation at concentrations upward of 15 mg/mL. Initial crystal trials were carried out in-house using commercial screens Clear Strategy I & 2, Morpheus, JCSG+ and PACT (Molecular Dimensions). These trials were conducted using the sitting drop vapour diffusion method in 96-well plates, with 400 nL droplets of both protein and reservoir solution. Further in-house trials were then conducted to screen around the condition, by both incubation of the protein sample with substrate prior to the trial, altering the concentrations of each reservoir component, and varying the overall pH of the reservoir solution.

NagB crystallization trials were also conducted at the C3 Collaborative Crystallography Center, based on hits in the in-house crystal trials that diffracted poorly when trialled at the beamline (8-9 Å). Here, two setups were developed to screen around a condition containing 0.2 M sodium citrate tribasic dehydrate, and 20% w/v polyethylene glycol (PEG) 3350. One setup was an additive screen, where various derivatives of sodium citrate were trialled, while systematically varying the % w/v of PEG 3350. The other setup was an additive screen where different salts were added to the condition in varying concentrations.

5.10.2 X-ray crystallography data collection

Preliminary X-ray data collection took place on the MX2 beamline at the Australian Synchrotron. Crystals were fished using cryo-loops and dipped in a cryoprotectant (85% of

the reservoir solution and 15% of a 1:1 ethylene glycol and glycerol solution) and then flash cooled in liquid nitrogen, before being mounted onto the beamline in a cold nitrogen stream at -173 °C.

References

Altamirano. (1993). Glucosamine-6-phosphate deaminase from Escherichia coli has a trimer of dimers structure with three intersubunit disulphides copy. *Biochem. J., 295*, 645-648.

Alvarez-Anorve, L. I., Gaugue, I., Link, H., Marcos-Viquez, J., Diaz-Jimenez, D. M., Zonszein, S., . . . Plumbridge, J. (2016). Allosteric Activation of Escherichia coli Glucosamine-6-Phosphate Deaminase (NagB) In Vivo Justified by Intracellular Amino Sugar Metabolite Concentrations. *J Bacteriol, 198*(11), 1610-1620. doi:10.1128/JB.00870-15

Borisova, M., Gaupp, R., Duckworth, A., Schneider, A., Dalugge, D., Muhleck, M., . . . Mayer, C. (2016). Peptidoglycan Recycling in Gram-Positive Bacteria Is Crucial for Survival in Stationary Phase. *MBio, 7*(5). doi:10.1128/mBio.00923-16

David, M. Z., & Daum, R. S. (2010). Community-associated methicillin-resistant Staphylococcus aureus: epidemiology and clinical consequences of an emerging epidemic. *Clin Microbiol Rev, 23*(3), 616-687. doi:10.1128/CMR.00081-09

Fischer, H., de Oliveira Neto, M., Napolitano, H. B., Polikarpov, I., & Craievich, A. F. (2009). Determination of the molecular weight of proteins in solution from a single small-angle X-ray scattering measurement on a relative scale. *Journal of Applied Crystallography, 43*(1), 101-109. doi:10.1107/s0021889809043076

Frieden, C. (1979). Slow transitions and hysteretic behavior in enzymes. *Annu Rev Biochem, 48*, 471-489. doi:10.1146/annurev.bi.48.070179.002351

Gordon, R. J., & Lowy, F. D. (2008). Pathogenesis of methicillin-resistant Staphylococcus aureus infection. *Clin Infect Dis, 46 Suppl 5*, S350-359. doi:10.1086/533591

Hall, R. S., Brown, S., Fedorov, A. A., Fedorov, E. V., Xu, C., Babbitt, P. C., . . . Raushel, F. M. (2007). Structural diversity within the mononuclear and binuclear active sites of N-acetyl-D-glucosamine-6-phosphate deacetylase. *Biochemistry, 46*(27), 7953-7962. doi:10.1021/bi700544c

Hall, R. S., Xiang, D. F., Xu, C., & Raushel, F. M. (2007). N-Acetyl-D-glucosamine-6-phosphate deacetylase: substrate activation via a single divalent metal ion. *Biochemistry, 46*(27), 7942-7952. doi:10.1021/bi700543x

Highlander, S. K., Hulten, K. G., Qin, X., Jiang, H., Yerrapragada, S., Mason, E. O., Jr., . . . Weinstock, G. M. (2007). Subtle genetic changes enhance virulence of methicillin resistant and sensitive Staphylococcus aureus. *BMC Microbiol, 7*, 99. doi:10.1186/1471-2180-7-99

Hiramatsu, K. (2001). Vancomycin-resistant Staphylococcus aureus: a new model of antibiotic resistance. *The Lancet Infectious Diseases, 1*(3), 147-155. doi:10.1016/s1473-3099(01)00091-3

Huang, Y. L., Chassard, C., Hausmann, M., von Itzstein, M., & Hennet, T. (2015). Sialic acid catabolism drives intestinal inflammation and microbial dysbiosis in mice. *Nat Commun, 6*, 8141. doi:10.1038/ncomms9141

Kanehisa, M., Sato, Y., Kawashima, M., Furumichi, M., & Tanabe, M. (2016). KEGG as a reference resource for gene and protein annotation. *Nucleic Acids Res, 44*(D1), D457-462. doi:10.1093/nar/gkv1070

Komatsuzawa, H., Fujiwara, T., Nishi, H., Yamada, S., Ohara, M., McCallum, N., . . . Sugai, M. (2004). The gate controlling cell wall synthesis in Staphylococcus aureus. *Mol Microbiol, 53*(4), 1221-1231. doi:10.1111/j.1365-2958.2004.04200.x

Kuznetsova, I. M., Turoverov, K. K., & Uversky, V. N. (2014). What macromolecular crowding can do to a protein. *Int J Mol Sci, 15*(12), 23090-23140. doi:10.3390/ijms151223090

Larkin, M. A., Blackshields, G., Brown, N. P., Chenna, R., McGettigan, P. A., McWilliam, H., . . . Higgins, D. G. (2007). Clustal W and Clustal X version 2.0. *Bioinformatics, 23*(21), 2947-2948. doi:10.1093/bioinformatics/btm404

Liu, C., Li, D., Liang, Y. H., Li, L. F., & Su, X. D. (2008). Ring-opening mechanism revealed by crystal structures of NagB and its ES intermediate complex. *J Mol Biol, 379*(1), 73-81. doi:10.1016/j.jmb.2008.03.031

Lunse, C. E., Schmidt, M. S., Wittmann, V., & Mayer, G. (2011). Carba-sugars activate the glmS-riboswitch of Staphylococcus aureus. *ACS Chem Biol, 6*(7), 675-678. doi:10.1021/cb200016d

McDonald, N. D., Lubin, J. B., Chowdhury, N., & Boyd, E. F. (2016). Host-Derived Sialic Acids Are an Important Nutrient Source Required for Optimal Bacterial Fitness In Vivo. *MBio, 7*(2), e02237-02215. doi:10.1128/mBio.02237-15

North, R. A. (2016). Bacterial sialic acid degradation: membrane transport and enzymology. *PhD Thesis*.

North, R. A., Kessans, S. A., Griffin, M. D., Watson, A. J., Fairbanks, A. J., & Dobson, R. C. (2014). Cloning, expression, purification, crystallization and preliminary X-ray diffraction analysis of N-acetylmannosamine-6-phosphate 2-epimerase from methicillin-resistant Staphylococcus aureus. *Acta Crystallogr F Struct Biol Commun, 70*(Pt 5), 650-655. doi:10.1107/S2053230X14007171

Oliva. (1995). Structure and catalytic mechanism of glucosamine 6-phosphate deaminase from Escherichia coli at 2.1 A resolution *Structure*.

Olson, M. E., King, J. M., Yahr, T. L., & Horswill, A. R. (2013). Sialic acid catabolism in Staphylococcus aureus. *J Bacteriol, 195*(8), 1779-1788. doi:10.1128/JB.02294-12

Owen, C. D., Lukacik, P., Potter, J. A., Sleator, O., Taylor, G. L., & Walsh, M. A. (2015). Streptococcus pneumoniae NanC: structural insights into the specificity and mechanism of a sialidase that produces a sialidase inhibitor. *J Biol Chem, 290*(46), 27736-27748. doi:10.1074/jbc.M115.673632

Petoukhov, M. V., Franke, D., Shkumatov, A. V., Tria, G., Kikhney, A. G., Gajda, M., . . . Svergun, D. I. (2012). New developments in the ATSAS program package for small-angle scattering data analysis. *J Appl Crystallogr, 45*(Pt 2), 342-350. doi:10.1107/S0021889812007662

Plumbridge, J. (2015). Regulation of the Utilization of Amino Sugars by Escherichia coli and Bacillus subtilis: Same Genes, Different Control. *J Mol Microbiol Biotechnol, 25*(2-3), 154-167. doi:10.1159/000369583

Rohmer, L., Hocquet, D., & Miller, S. I. (2011). Are pathogenic bacteria just looking for food? Metabolism and microbial pathogenesis. *Trends Microbiol, 19*(7), 341-348. doi:10.1016/j.tim.2011.04.003

Salton, M. R. J. (1964). Chemistry and function of amino sugars and derivatives. *Annu Rev Biochem*.

Sanchez, R., Serra, F., Tarraga, J., Medina, I., Carbonell, J., Pulido, L., . . . Dopazo, H. (2011). Phylemon 2.0: a suite of web-tools for molecular evolution, phylogenetics, phylogenomics and hypotheses testing. *Nucleic Acids Res, 39*(Web Server issue), W470-474. doi:10.1093/nar/gkr408

Somerville, G. A., & Proctor, R. A. (2009). At the crossroads of bacterial metabolism and virulence factor synthesis in Staphylococci. *Microbiol Mol Biol Rev, 73*(2), 233-248. doi:10.1128/MMBR.00005-09

Souza, J. M. (1997). NAcetylglucosamine-6-phosphate Deacetylase from Escherichia coli: Purification and Molecular and Kinetic Characterization. *Archives of Biochemistry and Biophysics*.

Suzuki, H., Tabata, K., Morita, E., Kawasaki, M., Kato, R., Dobson, R. C., . . . Wakatsuki, S. (2014). Structural basis of the autophagy-related LC3/Atg13 LIR complex: recognition and interaction mechanism. *Structure, 22*(1), 47-58. doi:10.1016/j.str.2013.09.023

Vimr, E. R. (2013). Unified theory of bacterial sialometabolism: how and why bacteria metabolize host sialic acids. *ISRN Microbiol, 2013*, 816713. doi:10.1155/2013/816713

Vincent, F., Davies, G. J., & Brannigan, J. A. (2005). Structure and kinetics of a monomeric glucosamine 6-phosphate deaminase: missing link of the NagB superfamily? *J Biol Chem, 280*(20), 19649-19655. doi:10.1074/jbc.M502131200

Vincent, F., Yates, D., Garman, E., Davies, G. J., & Brannigan, J. A. (2004). The three-dimensional structure of the N-acetylglucosamine-6-phosphate deacetylase, NagA, from Bacillus subtilis: a member of the urease superfamily. *J Biol Chem, 279*(4), 2809-2816. doi:10.1074/jbc.M310165200